Compatibility effect on stress-free two-way memory of Ni-Mn-Ga single crystal

Guoshun Qin[a], Chengguan Zhang[a], Shaobin Zhang[b], Xue Chen [c], Yongjun He[a, *]

[a]*UME, ENSTA Paris, Institut Polytechnique de Paris, 91120 Palaiseau, France*

[b]*School of Mechanics, Civil Engineering and Architecture, Northwestern Polytechnical University, Xi'an, China*

[c]*Faculty of Engineering and Environment, Northumbria University, Newcastle Upon Tyne, UK*

* Corresponding Author.

Email address: yongjun.he@ensta-paris.fr (Y. He)

Abstract:

A bar of single crystal Ni-Mn-Ga shape memory alloy takes the martensitic phase transformation via the nucleation and propagation of Austenite-Martensite (A-M) interfaces. Due to the compatibility between the two phases, very fine martensite twin laminates are generated near the A-M interface. Our experiments with the full-field observation on the specimen's non-uniform deformation by optical cameras and the meso-scale observation on the twin laminates by high-magnification microscopes reveal that the fine laminates after cooling are unstable and spontaneously evolve into a single martensite variant, i.e., the heating-cooling cycles trigger the material to switch between the austenite phase and one of the martensite variants with large cyclic deformations. Furthermore, to select the desired single variant among the possible martensite variants, we propose a special design—a single-crystal cantilever beam under mild heating-cooling cyclic thermal loading at its clamping end has two different parts: the part near the clamping end takes cyclic phase transformation while the other part near its free end keeps unchanged. Because of the compatibility requirement between the two parts, the cooled martensite state of the transformation part is governed by

the martensite state of the non-transformation part. That means, the compatibility relation can be adopted to design the cyclic deformation of the stress-free two-way memory.

Keywords: stress-free two-way memory, spontaneous martensite detwinning, martensitic phase transformation, microstructure compatibility, initial martensite state effect.

1. Introduction

Stress-free two-way memory with cyclic thermal-induced deformation has been intensively investigated for Shape Memory Alloys (SMAs) in the forms of polycrystal [1-5] and single crystal [6-11]. To build up the stress-free two-way memory in SMAs, some intentional training and/or thermo-mechanical treatments or unintentional operations of fabrication processes introduce microstructure defects and/or internal stresses which help choose some preferred martensite states and determine the output deformation during the cooling-induced phase transformation from austenite to martensite. In a very general sense, the stress-free cooling-induced martensite state can be a single martensite variant, a twin consisting of two martensite variants with proper relations, a simple mixture of multiple twins, or a self-accommodation configuration of multiple martensite variants without generating macroscopic shape change. Among all these possible states, the self-accommodation is usually assumed to describe the cooling-induced martensite configuration in untrained SMAs by most SMA researchers [5, 12-18]. However, referring to the experiments reported in literature, the self-accommodation martensite configuration appears in most normal SMA polycrystals, but it doesn't always appear in single crystals.

In literature, there are reports on the cooling-induced non-self-accommodated martensite with significant deformation strain in untrained SMA single crystals [19-22]. Because microstructure defects always exist and are unavoidable in real materials, those observations of the non-self-accommodated martensite states would probably be attributed to the defects which might be generated by unintentional operations of fabrication processes.

But it is not difficult to find another important factor governing the cooling-induced martensite state if we look into the mesoscopic and/or microscopic process of the phase transformation which always occurs via the nucleation and propagation of interfaces separating the two phases. For example, the interface between austenite and martensite (so-called A-M interface) can have different morphologies: arrow (wedge) [20, 23-24], X-type, λ-type [25-27] and simple planes [28-30]. These A-M interfaces can be nucleated at the boundaries of single-crystal specimens. For example, the theoretical discussion about the preference of the heating-induced austenite nucleation at the specimen's boundary rather than the specimen's inside can be found in [31]. Due to the compatibility requirements, the different A-M interface morphologies lead to different twins with various deformation strains. The cooling-induced martensite states generated via the nucleation and propagation of such interfaces can have non-accommodated twins as mentioned in [20]. That means, the existing experiments already imply that, due to the compatibility of the A-M interface, the stress-free two-way memory could be obtained in single crystal SMAs that switch between the austenite phase and the non-accommodated martensite phase during the heating-cooling cycles with significant deformation. But there are still several different non-self-accommodated martensite states (multiple twins, single twin, and a single martensite variant) which lead to different deformations in the heating-cooling cycles. For practical engineering applications of the two-way memory effect, a repeatable and predictable deformation is needed. So, a question naturally arises: can we predict and control the cooling-induced martensite state to achieve a reliable stress-free two-way memory?

In this paper, to utilize the A-M interface compatibility to control the two-way memory, we propose a special design—Incomplete Transformation System (ITS): a cantilever beam made from a single crystal SMA is *mildly* heated and cooled cyclically at its clamping end; thus, the part near the clamping end takes A↔M phase transformation cyclically while

the other part near its free end (being far from the heating-cooling clamping end) keeps the initial state without taking phase transformation. That means, the specimen (cantilever beam) has two parts(with and without phase transformation respectively) separated by an interface whose compatibility would determine (control) the two-way memory and the associated output deformation of the part taking the cyclic phase transformation.

In order to trace the evolution of the different martensite states and demonstrate clearly the compatibility relation, we choose a simple SMA single crystal: Ni-Mn-Ga whose room-temperature stable phase is martensite having approximately tetragonal symmetry with only 3 variants (M_1, M_2, and M_3) whose short axis "c" is along the coordinate "*x*", "*y*" and "*z*" respectively as shown in Fig. 1(a) [19, 32-36]. Although the magneto-mechanical coupling behaviours of Ni-Mn-Ga single crystal have been intensively studied [6, 26, 29, 30, 37-51], systematic detailed observations on the different A-M interface morphologies and the associated microstructure evolution during heating-cooling cycles have not yet been reported in literature.

When studying the compatibility effect on the ITS (cantilever beam being mildly heated and cooled), we observed a surprising phenomenon—Spontaneous Detwinning (SD): the cooling-induced martensite laminates of different martensite variants spontaneously evolved almost into a single martensite variant by merging the neighbouring twin boundaries. Moreover, the compatibility effect is highlighted in our several tests by setting different initial martensite states (M_1, M_2, and M_3) at the non-transformation part of the specimen (the part near the free end of the cantilever beam). The tests show that the cooling-induced martensite state of the transforming part always becomes the same state as the initial state of the non-transformation part. That means, we can control the deformation of the two-way memory of the beam's transforming part under mild heating-cooling cycles.

The remaining parts of this paper include the following sections: Section 2 describes the experimental procedures to observe both the global shape change and the meso-scale twin laminate structures in the cantilever beam. Section 3 reports the experiments comparing the behaviours of the ITS (cantilever beam under *mild* heating and cooling has a transformation part and a non-transformation part) with the Complete Transformation System (CTS: the whole cantilever takes phase transformation under *strong* heating and cooling). Then the conditions for the two-way memory and the associated spontaneous detwinning phenomenon are discussed in Section 4. Finally, the summary and conclusions are given in Section 5.

2. Material properties and experimental procedures

The specimens of $Ni_{50}Mn_{28}Ga_{22}$ (at. %) single crystal (from ETO Magnetic GmbH) are rectangular bars with all faces approximately along the {100} planes of the parent cubic austenite. The specimen's cross-section is2.5mm × 1mm, and its gauge length after clamping is around 10mm.The specimen has the characteristic phase transformation temperatures: M_f = 45 ^{o}C, M_s = 48 ^{o}C, A_s = 52 ^{o}C, A_f = 55 ^{o}C. As shown in Fig. 1(a), the martensite phase has a short axis $c \approx 0.561$ nm, two long axes $a \approx 0.595$ nm and the austenite phase has a characteristic length $a_0 \approx 0.584$ nm [48, 52]. So, with the reference of austenite, the martensite has the deformation strain of −4% along the short-axis direction and the deformation strain of +2% along the long-axis direction. The deformation strains of a martensite twin consisting of two different martensite variants can also be determined as shown in Appendix A. Strictly speaking, the material's martensite phase is slightly monoclinic with a 10M modulation, which allows the formation of various twin boundaries (e.g., Type I and Type II) and multiscale martensite structures (e.g., twins within twins) [53-56]. However, the tetragonal approximation was widely adopted to simplify the theoretical calculation and the discussion on the behaviours of the Ni-Mn-Ga single crystal [51, 57-59]. Here, the tetragonal approximation is also adopted to help understand the following macroscopic and mesoscopic

experiments. The effect of the approximation on the understanding of microscopic processes will be discussed at the end of Section 4 (Discussion Section).

The setup of the experiment is shown in Fig. 1(b) where a specimen is clamped at one end while the other end is free to deform. To monitor the deformation of the specimen, two optical cameras (CMOS: acA2000-340km, Basler, Germany) equipped with a Nikkor lens are used to observe the specimen's top surface (Camera 1) and one of the side surfaces (Camera 2). To observe the detailed deformation features of the Austenite-Martensite (A-M) interfaces, a microscope (AX70, Olympus, Japan) is adopted. Based on these optical observations and the technique of Digital Image Correlation (DIC of the software VIC-2D), the local strain distributions and in turn the distributions of the martensite variants can be determined (Appendix A). A thermocouple (K-Type of sheath diameter of 0.5 mm) is put at the clamping end to monitor the temperature evolution. The temperature at the clamping end can increase up to 60 ^{o}C for ITS (Incomplete Transformation System with mild heating) and up to 100 ^{o}C for CTS (Complete Transformation System with strong heating). Detailed procedures are presented as below.

CTS (Complete Transformation System with strong heating): A heater turns on to increase the temperature of the specimen's clamping end to about 100^{o}C to make the whole specimen take the austenite phase. Then, the heater turns off and the specimen's temperature decreases by natural cooling (i.e., by natural heat convection via the specimen's surfaces as shown in Figs. 2 and 3) or by ice cooling (i.e., by putting a block of ice at the specimen's clamping end as shown in Fig. 4). The different cooling modes lead to the nucleation and propagation of different A-M interfaces (with different orientations).

ITS (Incomplete Transformation System with mild heating): At the beginning of each test, the specimen takes martensite phase at room temperature (around 20 ^{o}C < M_f). The initial state of the whole specimen can be set to be a single martensite variant by mechanical

compression (i.e., the initial states M_1, M_2, and M_3 are set by mechanical compression along the *x*-, *y*-, and *z*-direction, respectively).The heater turns on to increase the temperature of the clamping end to near 60 ^{o}C; the A-M interface is nucleated and propagates from the clamping end to the middle of the specimen. Then, the heater turns off and the specimen's temperature decreases by natural cooling. Thus, the A-M interface propagates back from the middle to the clamping end and the final cooled martensite state of the whole specimen depends on the initial state we set at the beginning.

3. Experimental Results

Before reporting the behaviours of our special design (ITS) in Section 3.2, we demonstrate the general behaviours of a single crystal SMA bar via the CTS (the whole specimen taking phase transformation) under different cooling modes in Section 3.1.

3.1 CTS (whole specimen taking phase transformation)

When we strongly heated the clamping end (with the maximum temperature T_{max} near 100 °C), the whole specimen was transformed to austenite phase (A-phase), despite the initial martensite states at room temperature. Austenite (A-phase) is taken as the reference, i.e., zero strains $\varepsilon_{xx} = \varepsilon_{yy} = \varepsilon_{zz} = 0\%$ for A-phase as in the high-temperature state t_1 of Fig. 2 (note: t_1 represents the time, indicated by the temperature-time curve on the left-hand side in Fig. 2). As shown by the DIC strain maps at $t_2 \sim t_5$, when the heater was turned off, the specimen naturally cooled down to trigger the A → M phase transformation via the nucleation and growth of a martensite twin that consists of the martensite variants $M_3$and M_1whose volume ratio is 2:1(denoted as $M_3 : M_1$ twin)as the twin's deformation strains are $\varepsilon_{xx} \approx 0\%$, $\varepsilon_{yy} \approx 2\%$, and $\varepsilon_{zz} \approx -2\%$ (the method to determine the relation between the twin's deformation strains and the volume fractions of the two martensite variants can be found in Appendix A).

Because the average strain ε_{xx} of the twin M_3:M_1 is around zero, the transformation (A → twin M_3:M_1) has little contribution to the specimen's elongation (see t_1 ~ t_5 in the elongation-temperature curve in Fig. 2). It is also seen that the interface between the A-phase and the twin M_3:M_1 is almost parallel to the *x*-direction, which satisfies the compatibility requirement (detailed compatibility analysis can be found in Appendix B). When the twin grew to almost occupy the whole specimen (see the state t_5 of Fig. 2), a domain near the specimen's free end (at the position $x \approx 7$ mm) took the detwinning process (M_3:M_1 twin → M_3): the major component of the twin (i.e., M_3) grew at the expense of the minor component (M_1). Then, another detwinning domain appeared near the clamping end (see the states t_6 and t_7 of Fig. 2). The two domains of M_3 grew up and merged to occupy the whole specimen as shown in t_7 ~ t_{10} of Fig. 2, contributing to a significant elongation: the specimen's average ε_{xx} increased from 0% to nearly 1.6% as shown by the elongation-temperature curve in Fig. 2, indicating that the cooling-induced A → M phase transformation is via two steps: A →a twin (M_3:M_1) →a single variant (the twin's major component M_3).

While the first step (A → a martensite twin) is expected, the 2nd step (spontaneous detwinning) is totally out of expectation because martensite detwinning normally needs external driving forces, e.g., mechanical stress or magnetic field [29,39-42,48,49,51,53]. In order to confirm the existence of the spontaneous detwinning phenomenon, we improved our observation by a high-magnification microscope with polarized light and by polishing the specimen's surface. The detwinning process was recorded in Movie 1 (attached in the supplementary materials), and some frames of the movie are shown in Fig. 3. It is seen that the polarized light can significantly improve the observation by comparing Fig. 3(a) with Fig. 3(b). As shown in the observation with polarized light of Fig. 3(i), when austenite and martensite coexist, the compatibility of the two phases leads to the formation of a twin with very fine laminates (layers). After the A-M interface passes through the specimen (i.e.,

without the compatibility constraint), the fine laminates evolve by intermittent annihilation of the twin boundaries and the narrow laminae/layers finally become almost a single martensite variant. In fact, this spontaneous detwinning process can be theoretically explained: the high-energy state of the very fine twin laminates with numerous twin boundaries (causing lots of twin boundary energy) spontaneously evolves into the single martensite variant by the reduction of the surface energy (the energy of numerous twin boundaries). Some simple energetic analyses on the spontaneous detwinning and the description of different types of twin laminate structures can be found in our recent publication [60].

While the natural cooling mode (near homogeneous cooling) is demonstrated in Figs. 2 and 3, the ice cooling mode (i.e., inhomogeneous cooling with a thermal gradient along the specimen's length direction *x*-axis) is shown in Fig. 4 where the A-M interface is parallel to the specimen's width direction (*y*-axis). To afford such an interface, a twin M_3:M_2 (2:1) was formed with the strains ε_{xx} = 2%, ε_{yy} = 0%, and ε_{zz} = –2%, as shown in the strain maps at t_2 of Fig. 4. Because the twin had a tensile strain (ε_{xx} = 2%), the specimen's global elongation increased with the growth of the twin (see t_2 ~ t_5 of Fig. 4). Moreover, the spontaneous detwinning into single variant M_3 occurred at t_6 ~ t_{10} of Fig. 4.

By comparison between Figs. 2 and 4, it can be seen that the different cooling modes lead to different A-M interfaces of different orientations and different components of the twin (M_3:M_1 = 2:1 in Fig. 2 and M_3:M_2 = 2:1 in Fig. 4). But, for both twins, the spontaneous detwinning leads to the single variant M_3 as it occupies the main portion of both twins. Then, a doubt naturally rises: Does the specimen have very strong defects or internal stress to make the cooled martensite state prefer the single variant M_3? To eliminate this doubt, in the following tests of ITS (Incomplete Transformation System with mild heating), the initial state is set into different variants to check whether the cooled martensite is always M_3 (influenced

by the unknown defects) or depends on the initial state (governed by the compatibility relation).

3.2 ITS (Incomplete Transformation System with mild heating)

When the maximum heating temperature at the specimen's clamping end is not high (T_{max}near60^{o}C), the propagating A-M interface cannot reach the specimen's free end whose temperature is not high enough to take M→A transformation. So, such heating-cooling cycles make only a part of the specimen take cyclic phase transformation. At the beginning of each test (at room temperature), the initial martensite state of the specimen was set to be a single variant M_1, M_2, or M_3 as shown in the following Sections 3.2.1 to 3.2.3, respectively.

3.2.1: Initial state M_1

As shown in Fig. 5, at the beginning of the heating-cooling cycle, the specimen was occupied by M_1 whose strains are $\varepsilon_{xx} \approx -4\%$, $\varepsilon_{yy} \approx 2\%$, and $\varepsilon_{zz} \approx 2\%$ at t_1 and t_2. The heating triggered the nucleation and growth of the A-phase via a propagating A-M interface as shown by the strain maps at t_4 where the A-phase occupied around half of the specimen while the single martensite variant M_1 (the initial state) occupied the other part near the specimen's free end. When the heating was stopped and the specimen cooled down naturally with A-phase shrinking back and disappearing at the clamping end as shown by the strain maps at t_5~t_8, during which the part of the specimen near the clamping end changed to a martensite twin M_1:M_2 with the volume ratio 2:1 whose strains are $\varepsilon_{xx} \approx -2\%$, $\varepsilon_{yy} \approx 0\%$, and $\varepsilon_{zz} \approx 2\%$ (see the local strain maps/profiles). Then, the twin M_1:M_2 (2:1) spontaneously detwinned into the single variant $M_1$with the strains $\varepsilon_{xx} \approx -4\%$, $\varepsilon_{yy} \approx 2\%$, and $\varepsilon_{zz} \approx 2\%$ at t_8~t_{10}. The heating-cooling cycle makes the specimen's global elongation cyclically change between –3.4% and –1.4% (taking the specimen fully occupied by A-phase as the reference). That means the two-

way memory with a cyclic strain magnitude (around 2%) was achieved where around half of the specimen participated in the thermally induced cyclic A ↔ M_1phase transformation.

In order to see more clearly the feature of the A-M interface and the associated twin formation and detwinning, we repeated the above test by three continuous heating-cooling cycles with the meso-scale observation by a microscope shown in Figs. 6-8 respectively. During the heating of the 1st cycle (Fig. 6), the triangular transition zone consisting of twin M_1:M_2 (with volume ratio 2:1 whose average strains were $\varepsilon_{xx} \approx -2\%$ and $\varepsilon_{yy} \approx 0\%$) was observed between the A-phase and the single variant M_1(see the DIC strain maps (i) ~ (vi));by contrast, during the cooling, the transition zone (twin M_1:M_2) grew up at the expense of A-phase (see (vii)~(xi)) which agreed with the full-field DIC strain maps of the whole specimen (states t_5~t_8 in Fig. 5 where the transition zone also grew up). Finally, the twin evolved into the single variant M_1 (see (xi) and (xii) in Fig. 6). However, the twin M_1:M_2 is just one of the possible configurations of the transition zone for separating the A-phase from the single variant M_1; the heating process of the 2nd cycle shows another configuration of the transition zone (see (i)~(v) in Fig. 7): the triangular transition zone consisting of twin M_1:M_3 (with volume ratio 2:1 whose average strains are $\varepsilon_{xx} \approx -2\%$ and $\varepsilon_{yy} \approx 2\%$). With the magnified view in Fig. 7, we can see that the transition zone is a fine laminate. More interesting is that, during cooling-induced A→M transformation, the transition zone changed to the twin M_1:M_2 (2:1) as shown in (vii)~(xii) where the A-phase shrank while the transition zone M_1:M_2 grew up and was detwinned into M_1 simultaneously. It is easy to apply a compatibility analysis to verify that both the twin M_1:M_2 (2:1) and the twin M_1:M_3 (2:1) can be compatible with A-phase (see Appendix B).In fact, these two twins can co-exist at the transition zone as shown in the heating process of the 3rd cycle (see (i)~(iv) in Fig. 8) where an “X” type interface was observed. But, in the cooling process, only one twin appeared (M_1:M_2) which detwinned into M_1 as shown in (vii)~(xii) of Fig. 8.

The above observations show that the A-M interface can be composed by only one plane (with only one twin at the transition zone) or by multiple planes (with multiple twins at the transition zone). The various interfacial microstructures (X-type, λ-type, and the associated twins within twins) were well discussed in [27, 61-63]. In order to double-check the existence of the X-type A-M interface in the current system, we repeated the above heating-cooling cycle on the specimen after polishing; the propagation of the X-type A-M interface during the heating process was recorded in Movie 2 (in supplementary materials). A typical picture from the movie and the schematic of the associated twins are shown in Fig. 9. Based on the theoretical analysis on the compatible A-M interfaces and the associated twins in Appendix B, the components of the twins in Fig. 9 can be identified by the observed orientations of the A-M interfaces and twin boundaries. From the comparison between the theoretical predictions and the experimental observation, Fig. 9(b) schematically demonstrates the interfaces/boundaries OP_1, OP_2, OP_3, and OP_4, separating the four domains: A-phase, twin M_1:M_2, twin M_1:M_3, and the single variant M_1. One point that might be important to point out is that, in all of our tests, the stable propagation of the X-type interface only appears in the heating-induced M→A process. The reason might be related to the different kinetics of the forward and reverse martensitic phase transformations during the heating-cooling cycles, which need further study.

3.2.2: Initial state M_2

To further verify the initial-state effect, we repeated the above heating-cooling cycle on the specimen with a different initial martensite state: the single martensite variant M_2 whose strain components are $\varepsilon_{xx} \approx 2\%$, $\varepsilon_{yy} \approx -4\%$, and $\varepsilon_{zz} \approx 2\%$ (achieved by compression along *y*-direction). As shown in Fig. 10, the specimen after the heating-cooling cycle returned to the same martensite variant as the initial state M_2 with the cyclic global elongation between

1% and 2% (see the DIC strain maps t_1~t_{10} and the elongation-temperature curve). Different from the observed transition zone in Section 3.2.1, the current transition zone between A-phase and the single variant M_2 is a twin M_2:M_3 (with the volume ratio 2:1 whose average strain components are $\varepsilon_{xx} \approx 2\%$, $\varepsilon_{yy} \approx -2\%$, and $\varepsilon_{zz} \approx 0\%$) as shown in the strain maps and the strain profiles at $t_6 \sim t_8$ in Fig. 10. Clearer pictures of the transition zone are shown in Fig. 11 about the observation by the microscope. It is seen, in the strain maps (ii) ~ (iv) during the heating and (viii) ~ (x) during the cooling, that the transition zone has some coarse spikes (arrows) pointing to the region of the single variant M_2 while the boundary between A-phase and the transition zone is quite smooth, which in fact is a laminate of fine twins M_2:M_3 as shown by the magnified view in Fig. 11.

3.2.3: Initial state M_3

To complete the study on the initial-state effect, the same heating-cooling cycle was also performed with the initial martensite state M_3 as shown in Fig. 12 where the response is similar to that with the initial state of M_2 in Fig. 10 in Section 3.2.2: both make the specimen elongation positive (i.e., tensile strain along the specimen's length direction *x*-axis)because the atomic lattices of both M_2 and M_3 have a long axis along the *x*-direction, which is a contrast to the case of the initial state M_1in Fig. 5 of Section 3.2.1 where the specimen's elongation is negative. Moreover, the composition of the transition zone in Figs.10 and 12arealmostthe same—a combination of M_2 and M_3, but with a different volume ratio—the twin M_3:M_2=2:1 for the initial state M_3 (see state t_6 in Fig. 12) while the twin M_2:M_3=2:1 for the initial state M_2 (see state t_7 in Fig. 10). Comparing these compositions with those for the initial state M_1 (M_1:M_2=2:1 or M_1:M_3=2:1 in Fig. 2), we can see that the initial state (the single variant in the untransformed region of the beam's free end) is always the major

component of the twin in the transition zone, and it would be the final cooled martensite state after the spontaneous detwinning.

4. Discussion

Although the unavoidable material microstructure defects might have an influence on the martensitic phase transformation, the above experimental results clearly demonstrate the strong governing factor—compatibility: all the twins generated at the A-M interfaces with various orientations are always among the six compatible compositions, M_1:M_2, M_1:M_3, and M_2:M_3 with the volume ratios 2:1 or 1:2 (Details of the relation of the orientations between the twin boundaries and the A-M interfaces can be found in Table B1 and Fig. B1 of Appendix B). That means, the six compatible twins are the only possible cooled martensite states. Moreover, if the A-M interface sweeping the specimen is a planar interface, only one of the six twins can exist. Furthermore, when the A-M interface disappears (or the twin is located far from the compatibility constraint of the A-M interface), the twin can automatically evolve almost into a single martensite variant, leading to the significant deformation of the stress-free two-way memory.

In all the above spontaneous detwinning processes, the major component of the twin (i.e., the martensite variant with the volume fraction 2/3) always grows at the expense of the minor component (i.e., the martensite variant with the volume fraction 1/3). That can be easily understood with the simple schematic in Fig. 13. The nearest neighbouring twin boundaries move to each other, merge together and finally disappear, making the whole region of the original twin becomes a single martensite variant (the major component of the original twin). It should be noted that the current Ni-Mn-Ga single crystal is a ferromagnetic SMA which is sensitive to external magnetic fields [29, 30, 33, 35, 43, 44]. So, the current experimental setup contains only non-magnetic devices (e.g., the clamping devices are made from

aluminium) and the experiments are performed far away from any magnetic equipment. That is to say, spontaneous detwinning occurs without external mechanical stress or magnetic field.

The compatibility effect is much highlighted in our special design ITS (a cantilever beam under mild heating-cooling cycles) which has a transformation part and a non-transformation part. For example, as shown in the DIC strain map (ix) of Fig. 6, the transition zone (M_1:M_2) between the two domains (A-phase and the single variant M_1) has to be compatible with both domains. As shown in the schematic of Fig. 14, while the volume ratio 2:1 of the two components (M_1 and M_2) makes the twin compatible with A-phase at the interface "P_1P_2", the twin boundaries parallel to the interface "P_3P_4" naturally make the twin compatible with the single variant M_1. More interesting is that, in all the above observations on the coexistence of three domains (A-phase, a twin and a single variant), the single variant is always the major component of the twin. Based on the above discussions, we can understand why the initial state (a single martensite variant) of the non-transformation part near the beam's free end can determine the final cooled martensite state of the transformation part near the beam's clamping end. Due to the compatibility of the three domains, the twin's major component is the initial state of the non-transformation part; the twin occupies the transformation part at the end of the cooling process, and then spontaneously evolves into its major component (i.e., the initial state of the beam's free end) making the two-way memory predictable and controllable.

For understanding the implications of the current experiments, it would be helpful to compare the current experimental observations on the Ni-Mn-Ga single crystal with the general behaviours of SMAs during the thermally induced martensitic phase transformation. As polycrystals are adopted in most engineering applications of SMAs, their behaviours have been well studied; particularly it has been revealed by experiments and modelling [64-67] that the thermally induced martensitic phase transformation can generate self-accommodated

martensite structures: triangular or diamond-like patterns consisting of different martensite variants within the grains due to the constraints from the grain boundaries and the interactions with the neighbouring grains. The self-accommodation mechanism makes the global shape of the polycrystals unchanged during the phase transformation. Therefore, the SMA polycrystals without training or special microstructures/defects would not have stress-free two-way memory. By contrast, SMA single crystals can have non-self-accommodated martensite structures leading to the shape change during cooling, especially when the phase transformation starts at the specimen's boundary (i.e., without the environmental constraint like the grain boundaries in polycrystals) [19-22]. It is interesting to note that our material (Ni-Mn-Ga) with cubic austenite and approximately volume-preserving martensitic phase transformation satisfies the necessary and sufficient conditions for self-accommodation according to the reference [73], but the cooling-induced martensite with large deformation is obviously non-self-accommodation in our experiments (see the elongation-temperature curves of in Figs. 2, 4 and 5). The reason might be that the nucleation of martensite in our experiments occurs at the specimen's surfaces/edges rather than inside the specimen. By contrast, the reference [73] mainly concerns the martensite nucleation in "the sea of austenite"—the nucleated martensite is surrounded by a sea of austenite on all sides. That means, even though the material's symmetry and lattice parameters satisfy the conditions for self-accommodation, the single crystals can choose non-self-accommodation by nucleating martensite at free boundaries (specimen's surfaces/edges).

The current experiment on the cantilever beam of the Ni-Mn-Ga single crystal not only gives an example of the non-self-accommodated martensite structure (very fine twin laminates) but also captures the spontaneous detwinning process making the twin laminates evolve into the "single martensite variant" to provide a large global deformation during cooling. Here the "single martensite variant" means a tetragonal martensite variant which is

an approximation of the slightly monoclinic martensite variant (Ni-Mn-Ga with 10M modulation) that has not only the short axis (c-axis), but also two different long axes (a and b axes) and the characteristic angle 90.37^{o} [55]. It has been revealed that the monoclinic martensite variants can form complicated multi-scale martensite structures with the lower-scale twins (e.g., modulation twin [54] and a/b twins [56]). A simple example of the multiscale martensite structures (a/b twins within macro-twins) is sketched in Fig. 15(a). It is seen that the macro-twin boundary (1st-order twin boundary) separates the domains with different orientations of the c-axis; within each domain, there are 2nd-order twin boundaries separating the sub-domains of different orientations of the long axes (a and b axes). So, the "single martensite variant" demonstrated in the above DIC strain maps in t_{10} of Fig. 2 and (xii) of Fig. 7 should have numerous sub-domains that could be revealed by microscopic observation facilities with higher resolution. Moreover, the microstructure would become much more complicated when the magnetic influence is taken into account in the current material (Ni-Mn-Ga magnetic SMA).

It has been revealed by both experiments and modelling [68-71] that the magnetic domains can be embedded in the martensite twins of the magnetic SMAs as schematically shown in Fig. 15(b) where the macro twin boundary (1st-order twin boundary) and the 90^{o} domain wall are overlapped. It is implied that the magnetic energy (particularly the90^{o} domain wall formation/evolution) would influence the surface energy and the mobility of the macro twin boundary. That might be the reason for the current material to have some special behaviour different from other non-magnetic SMAs. To the best knowledge of the authors, there are no experiments or models able to clearly describe the magnetic domains embedded in the multiscale twins by the combination of Fig. 15(a) and (b) that would provide physical insights into the kinetics of the magnetic domains and the twin evolution (e.g., the correlation

between the movement of the multiscale twin boundaries and the movement of the different domain walls and the associated magnetization rotation).

In a nutshell, while the non-self-accommodating twin laminates generated by the thermally induced phase transformation in SMA single crystals are not surprising, the current experiments on the Ni-Mn-Ga single crystal demonstrate an unexpected spontaneous detwinning process making the twin laminates evolve into “single martensite variant” which so far has not been observed in other SMA single crystals; the reason might be related to the high mobility of the twin boundary and the associated magneto-mechanical coupling within the multiscale martensite structure correlated with the magnetic domains.

5. Summary and conclusions

The stress-free two-way memory and the associated compatibility effects are demonstrated in a cantilever beam of SMA single crystal which takes full transformation (CTS in Section 3.1) and partial transformation (ITS in Section 3.2) with different initial states under different cooling modes (natural cooling and ice cooling). With the help of the optical cameras, the microscopes and the DIC technique (determining the distributions of the local deformation strains), it is revealed that the compatibility always governs the phase transformation processes with the compatible A-M interfaces and the associated twins’ formation and evolution leading to the two-way memory. Although the current material under study (Ni-Mn-Ga single crystal) is assumed to have simple symmetry (tetragonal symmetry), the experiences and the concepts from the study could be extended to other materials. Two major conclusions can be drawn from the study:

1. When the martensitic phase transformation under cooling occurs via the nucleation and propagation of a planar A-M interface, the final cooled martensite state is achieved by

two steps: (1) austenite→a twin; (2) detwinning into single martensite variant. The major component of the twin is the final martensite state.

2. The compatibility between the three domains (austenite phase, a martensite twin and a single martensite variant) makes the stress-free two-way memory predictable and controllable when only part of the specimen takes the cyclic phase transformation under heating-cooling cycles.

Appendix A Determination of twin's composition via local strains

The three martensite variants M_1, M_2 and M_3 with their short axes along x, y and z respectively are shown in Fig.1(a) where the variant's short axis $c \approx 0.561$ nm, long axis $a \approx 0.595$ nm and the austenite characteristic length $a_0 \approx 0.584$ nm. Therefore, the martensite variants have the deformation strains of –4% and +2% along their short- and long-axis directions respectively, taking austenite phase as the reference. That means the characteristic transformation strains of the three variants are: M_1 ($\varepsilon_{xx} \approx -4\%$, $\varepsilon_{yy} \approx 2\%$, and $\varepsilon_{zz} \approx 2\%$), M_2 ($\varepsilon_{xx} \approx 2\%$, $\varepsilon_{yy} \approx -4\%$, and $\varepsilon_{zz} \approx 2\%$) and M_3 ($\varepsilon_{xx} \approx 2\%$, $\varepsilon_{yy} \approx 2\%$, and $\varepsilon_{zz} \approx -4\%$). As shown by the DIC strain maps in Figs. 2, 4~8 and 10~12, some regions of the specimen are not transformed to these three single variants, but their combinations. So, we need to determine the volume fractions of M_1, M_2 and M_3 (denoted as f_1, f_2 and f_3) based on the measured local strain components. At the temperature lower than the characteristic phase transformation temperature M_f, the material is in martensite state; so there is a relation between f_1, f_2 and f_3:

$$f_1 + f_2 + f_3 = 1 \tag{A1}$$

Usually two principle strain components can be measured by one camera; for example, the DIC strain maps and profiles of surfaces observed by Camera 1 in Fig. 2 or by a microscope in Fig. 6 showing the two components ε_{xx} and ε_{yy} of the local strains. Two equations can be derived from these two strain components:

$$\begin{cases} -0.04 f_1 + 0.02 f_2 + 0.02 f_3 = \varepsilon_{xx} & \text{(A2)} \\ 0.02 f_1 - 0.04 f_2 + 0.02 f_3 = \varepsilon_{yy} & \text{(A3)} \end{cases}$$

Combining Eqs. (A1), (A2) and (A3), we obtain the volume fractions:

$$\begin{cases} f_1 = \dfrac{0.02 - \varepsilon_{xx}}{0.06} \\ f_2 = \dfrac{0.02 - \varepsilon_{yy}}{0.06} \\ f_3 = \dfrac{0.02 + \varepsilon_{xx} + \varepsilon_{yy}}{0.06} \end{cases} \quad (A4)$$

Similarly, for the two components ε_{xx} and ε_{zz} of the strain mapsmeasured by Camera 2 in Fig. 2, two equations can be derived:

$$\begin{cases} -0.04 f_1 + 0.02 f_2 + 0.02 f_3 = \varepsilon_{xx} & (A5) \\ 0.02 f_1 + 0.02 f_2 - 0.04 f_3 = \varepsilon_{zz} & (A6) \end{cases}$$

By solving equations (A1), (A5) and (A6), the volume fractions can be obtained:

$$\begin{cases} f_1 = \dfrac{0.02 - \varepsilon_{xx}}{0.06} \\ f_2 = \dfrac{0.02 + \varepsilon_{xx} + \varepsilon_{zz}}{0.06} \\ f_3 = \dfrac{0.02 - \varepsilon_{zz}}{0.06} \end{cases} \quad (A7)$$

Example: The strain maps of (iii) in Fig.6 show that, between A-phase and the single variant M_1, there is a triangular transtional zone with the strain components $\varepsilon_{xx} \approx -2\%$, $\varepsilon_{yy} \approx 0\%$. Then, Eq. (A4) gives the volume fractions: $f_1 = 2/3$, $f_2 = 1/3$ and $f_3 = 0$. Therefore, this transition zone consists of only two variants M_1 and $M_2$with the volume ratio 2:1, denoted as M_1:M_2 (2:1).

Appendix B Compatible austenite-twin interfaces

The following compatibility analysis is based on the previous results in [51,72]. The Bain matrix of the three different tetragonal variants M_1, M_2 and M_3 (whose short axes respectively along *x*, *y* and *z*) are:

$$U_1=\begin{pmatrix}\alpha & 0 & 0\\ 0 & \beta & 0\\ 0 & 0 & \beta\end{pmatrix},\quad U_2=\begin{pmatrix}\beta & 0 & 0\\ 0 & \alpha & 0\\ 0 & 0 & \beta\end{pmatrix},\quad U_3=\begin{pmatrix}\beta & 0 & 0\\ 0 & \beta & 0\\ 0 & 0 & \alpha\end{pmatrix}$$

where $\beta = \frac{a}{a_0} = 1.0188$ and $\alpha = \frac{c}{a_0} = 0.9606$ (a, c and a_0 are the lattice paremeters of the material as shown in Fig. 1(a)). The compatible interfaces between the austenite phase and the martensite twins can be obtained by solving the following two equations, so-called twinning equation and the austenite-martensite interface equation:

$$\begin{cases} QU_j - U_i = a \otimes n & \text{(B1)} \\ Q'(\lambda QU_j + (1-\lambda)U_i) = I + b \otimes m & \text{(B2)} \end{cases}$$

where $\boldsymbol{U_i}$ and $\boldsymbol{U_j}$ are the Bain matrix of the i^{th} and the j^{th} martensite variants; $\boldsymbol{I}$ is an identity second-order tensor representing the Bain matrix of the A-phase; $\boldsymbol{Q}$ represents the rotation of the variant $\boldsymbol{U_j}$ with respect to the variant $\boldsymbol{U_i}$ when the twin is formed; $\boldsymbol{Q'}$ represents the rotation of the martensite twin (consisting of the i^{th} and the j^{th} martensite variants) with respect to the A-phase; $a \otimes n$ is a dyadic product of a non-zero vector $\boldsymbol{a}$ and a unit vector $\boldsymbol{n}$; the vector $\boldsymbol{n}$ represents the normal of the twinning plane in the reference cubic coordinate system while the vector $\boldsymbol{a}$ is the shearing vector. $\boldsymbol{m}$ is the normal of the A-M interface while the vector $\boldsymbol{b}$ is the shear vector; λ and $(1-\lambda)$ are the fractions of the j^{th} and the i^{th} martensite variants.

The approximatedsolutions to the two equations provide all the possible compatible interfaces between austenite phase and martensite twins that are listed in Table B1, and

schematically drawn in Fig. B1 for the *x-y* plane that were observed by Camera 1 and by the microscope in the experimental results in Figs. 2 ~ 14.

Martensite variant pair $M_i:M_j$	λ (fraction of M_i)	$\boldsymbol{n}$ (normal of fine twin)	$\boldsymbol{m}$ (normal of A-M interface)	Trace of A-M interface (on observation surface)
$M_1:M_3$	32%	$\frac{1}{\sqrt{2}}[1\ 0\ 1]$	$\frac{1}{\sqrt{2}}[0\ 1\ \pm1]$	horizontal (Fig. B1(a))
		$\frac{1}{\sqrt{2}}[1\ 0\ -1]$	$\frac{1}{\sqrt{2}}[0\ 1\ \pm1]$	
	68%	$\frac{1}{\sqrt{2}}[1\ 0\ 1]$	$\frac{1}{\sqrt{2}}[\pm1\ 1\ 0]$	45° (Fig. B1(b))
		$\frac{1}{\sqrt{2}}[1\ 0\ -1]$	$\frac{1}{\sqrt{2}}[\pm1\ 1\ 0]$	
$M_1:M_2$	32%	$\frac{1}{\sqrt{2}}[1\ 1\ 0]$	$\frac{1}{\sqrt{2}}[0\ \pm1\ 1]$	horizontal (Fig. B1(c))
		$\frac{1}{\sqrt{2}}[-1\ 1\ 0]$	$\frac{1}{\sqrt{2}}[0\ \pm1\ 1]$	
	68%	$\frac{1}{\sqrt{2}}[1\ 1\ 0]$	$\frac{1}{\sqrt{2}}[\pm1\ 0\ 1]$	vertical (Fig. B1(d))
		$\frac{1}{\sqrt{2}}[-1\ 1\ 0]$	$\frac{1}{\sqrt{2}}[\pm1\ 0\ 1]$	
$M_3:M_2$	32%	$\frac{1}{\sqrt{2}}[0\ 1\ 1]$	$\frac{1}{\sqrt{2}}[1\ \pm1\ 0]$	45° (Fig. B1(e))
		$\frac{1}{\sqrt{2}}[0\ -1\ 1]$	$\frac{1}{\sqrt{2}}[1\ \pm1\ 0]$	
	68%	$\frac{1}{\sqrt{2}}[0\ 1\ 1]$	$\frac{1}{\sqrt{2}}[1\ 0\ \pm1]$	vertical (Fig. B1(f))
		$\frac{1}{\sqrt{2}}[0\ -1\ 1]$	$\frac{1}{\sqrt{2}}[1\ 0\ \pm1]$	

Table B1 Theroretical compatible interfaces between austenite phase and martensite twins

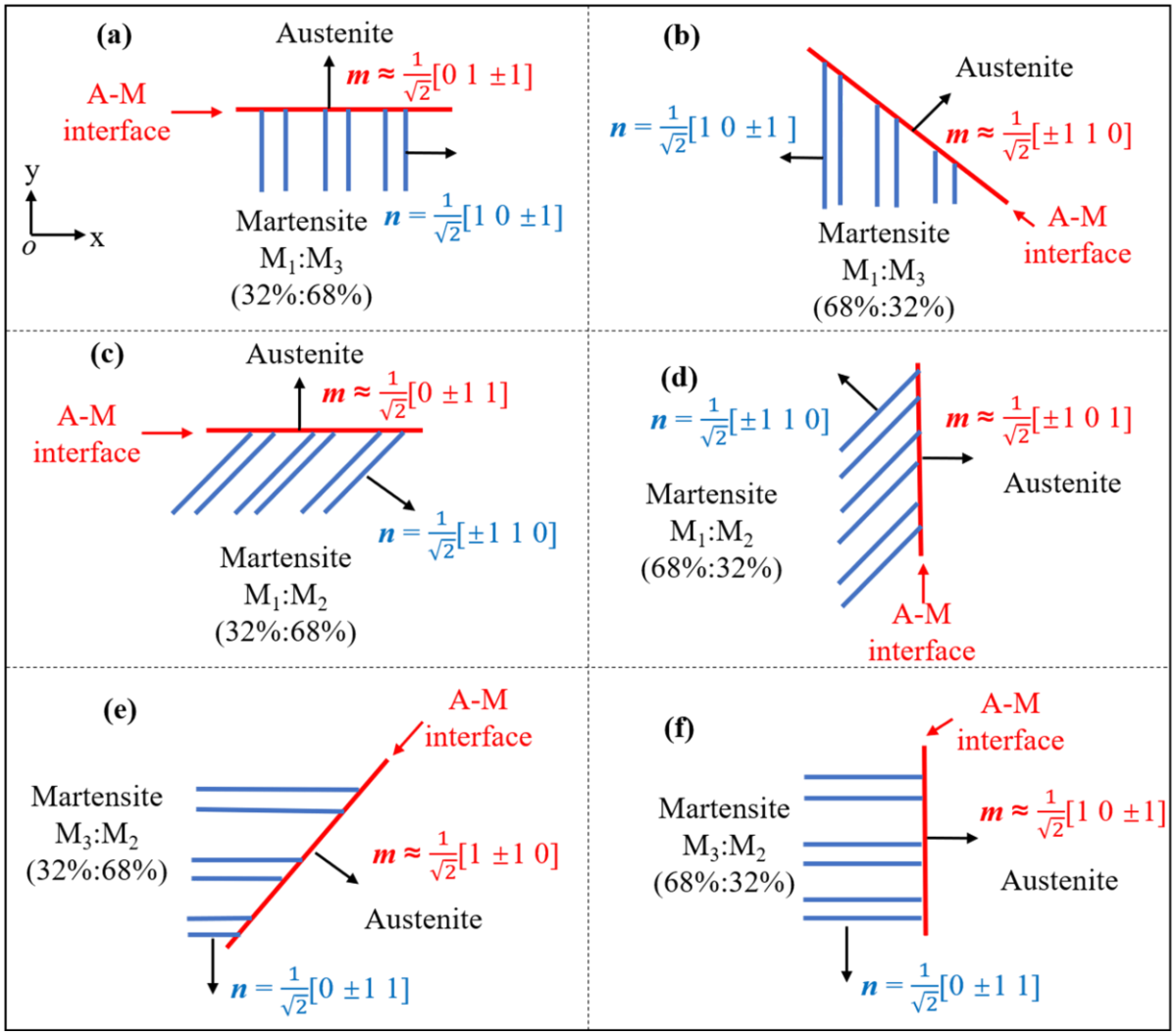

Fig. B1 The schematics of the theroretical compatible interfaces between austenite phase and martensite twins

In case we need the accurate orientations of the A-M interface for comparison with very precise experiments, the procedures in [72] to obtain the accurate solutions of Eqs. (B1) and (B2) can be adopted. For example, the following formula Eq. (B3) can be used to determine the orientation (the vector $\boldsymbol{m}$) of the A-M interface compatible with a martensite twin.

$$\boldsymbol{m}^{\pm} = \frac{1}{\rho}\left\{\mp\frac{\delta+\tau}{2}, \pm\frac{\delta-\tau}{2}, 1\right\}$$

$$\delta = \sqrt{\frac{\alpha^2+\beta^2-2}{1-\alpha^2}}, \quad \tau = \sqrt{\frac{2\alpha^2\beta^2-\alpha^2-\beta^2}{1-\alpha^2}} \qquad \text{Eq. (B3)}$$

With the parameters of the tetragonal martensite variant, $\beta =$ 1.0188 and $\alpha =$ 0.9606 , the vector $\boldsymbol{m}$ can be expressed:

$$\boldsymbol{m} \approx [\pm 0.7253\ \ \pm 0.0252\ \ 0.6879]$$

$$= \frac{1}{\sqrt{2}} [\pm 1.0257 \ \pm 0.0356 \ \ 0.9728]$$

$$\equiv \frac{1}{\sqrt{2}} [m_x \ m_y \ m_z] \qquad \text{Eq. (B4)}$$

This calculated vector $\boldsymbol{m}$ is close to that in [57] where $\boldsymbol{m} = \frac{1}{\sqrt{2}} [-1.05 \ -0.03 \ \ 0.94]$. Considering that $|m_x| = 1.0257 \approx 1$, $|m_y| = 0.0356 \approx 0$, and $|m_z| = 0.9728 \approx 1$, we obtain the approximated vector $\boldsymbol{m} \approx \frac{1}{\sqrt{2}} [\pm 1 \ \ 0 \ \ 1]$.

References:

[1] P. Larochette, E. Cingolani, A. Yawny, M. Ahlers, The two way shape memory effect in stabilized Cu-Zn-A1 single and polycrystals, J. phys. IV 7(1997) 495-500.

[2] R.Stalmans, J.Van Humbeeck, L.Delaey,The two way memory effect in copper-based shape memory alloys--thermodynamics and mechanisms, Acta metall. mater. 40(1992) 2921-2931.

[3] J. Su, W. Huang, M. Hong, Indentation and two-way shape memory in a NiTi polycrystalline shape-memory alloy, Smart Mater. Struct. 16(2007) S137.

[4] J. Sui, X. Zhang, X. Zheng, Z. Yang, W. Cai, X. Tian,Two-way shape memory effect of polycrystalline Ni-Mn-Ga-Gd high-temperature shape memory alloys,Scripta Mater. 68(2013)679-682.

[5] L. Xu, A. Solomou, T. Baxevanis, D. Lagoudas, Finite strain constitutive modeling for shape memory alloys considering transformation-induced plasticity and two-way shape memory effect, Int. J. Solids Struct. 221(2021) 42-59.

[6] M.Chmielus, V.A. Chernenko, W.B. Knowlton, G. Kostorz, P. Müllner,Training, constraints, and high-cycle magneto-mechanical properties of Ni-Mn-Ga magnetic shape-memory alloys, Eur. Phys. J. Spec. Top. 158(2008) 79-85.

[7] A. Eftifeeva, E. Panchenko, Y. Chumlyakov, H. J. Maier, Two-way shape memory effect in $[001]_{B2}$-oriented Co-Ni-Al single crystals, Mater. Today: Proc. 4(2017) 4789-4796.

[8] E. Panchenko, A. Eftifeeva, Y. Chumlyakov, G. Gerstein, H.J. Maier, Two-way shape memory effect and thermal cycling stability in $Co_{35}Ni_{35}Al_{30}$ single crystals by low-temperature martensite ageing, Scripta Mater. 150(2018) 18-21.

[9] C. Picornell, E. Cesari, M. Sade, Characteristics of the martensitic transformation and the induced two-way shape memory effect after training by compressive pseudoelastic cycling in Cu-Zn-Al single crystals, Metall. Mater. Trans. A 25(1994) 687-695.

[10] W. H.Wang, G. H.Wu, J. L. Chen, C. H.Yu, S. X. Gao, W. S. Zhan, Stress-free two-way thermoelastic shape memory and field-enhanced strain in $Ni_{52}Mn_{24}Ga_{24}$ single crystals, Appl. Phys. Lett. 77(2000) 3245.

[11] Y.Zhao, J. Xue, Y. Zhang, M. Kang, H. Gao, J. Wang, Two-way shape memory effect and magnetic-field-induced twin boundary motion in Ni-Mn-Ga microwire, Mater. Lett. 243(2019)173-175

[12] Y.Chemisky, A.Duval, E. Patoor, T. Ben Zineb, Constitutive model for shape memory alloys including phase transformation, martensitic reorientation and twins accommodation, Mech. Mater. 43(2011) 361-376.

[13] J.P.Hirth, R.C. Pond, Compatibility and accommodation in displacive phase transformations, Prog. Mater. Sci. 56(2011) 586-636.

[14] K.Madangopal, The self accommodating martensitic microstructure of Ni-Ti shape memory alloys, Acta Mater. 45(1997) 5347-5365.

[15] K.Madangopal, J.Singh, S. Banerjee, Self-accommodation in Ni-Ti shape memory alloys,Scripta Metall. Mater. 25(1991) 2153-2158.

[16] K. Madangopal, J.B. Singh, S. Banerjee, The nature of self-accommodation in Ni-Ti shape memory alloys, Scripta Metall. Mater. 29(1993) 725-728.

[17] K. Madangopal, R. Tiwari, S. Banerjee, Microscopic self-accommodation in shape memory alloy martensites, Scripta Metall. Mater. 28(1993) 991-996.

[18] T. Teramoto, K. Nagahira, K. Tanaka, Geometry and energy barrier of martensite in the initial stage martensitic transformation in B19’ TiNi shape memory alloy, Acta Mater. 201(2020) 94-101.

[19] V. Pinneker, M. Gueltig, A. Sozinov, M. Kohl, Single phase boundary actuation of a ferromagnetic shape memory foil, Acta Mater. 64(2014) 179-187.

[20] S.Tan, H. Xu, Observations on a CuAlNi single crystal, Continuum Mech. Therm. 2(1990) 241-244.

[21] F.Xiong, Y. Liu, Thermomechanical stability of Ni-Mn-Ga single crystal,Mater. Sci. Eng. A432(2006) 178-183.

[22] B. Yuan, X. Zhu, X. Zhang, M. Qian, Elastocaloric effect with small hysteresis in bamboo-grained Cu-Al-Mn microwires, J. Mater. Sci. 54(2019) 9613-9621.

[23] X. Balandraud, G. Zanzotto, Stressed microstructures in thermally induced M9R-M18R martensites, J. Mech. Phys. Solids. 55(2007) 194-224.

[24] K.Bhattacharya, Wedge-like microstructure in martensites, Acta Metall. Mater.39(1991) 2431-2444.

[25] H. Seiner, Mobile interfacial microstructures in single crystals of Cu-Al-Ni shape memory alloy, Shap. Mem. Superelasticity 1(2015) 268-274.

[26] H. Seiner, O. Glatz, M. Landa, A finite element analysis of the morphology of the twinned-to-detwinned interface observed in microstructure of the Cu-Al-Ni shape memory alloy, Int. J. Solids Struct. 48(2011) 2005-2014.

[27] H. Seiner, P. Sedlák, M. Landa, Shape recovery mechanism observed in single crystals of Cu-Al-Ni shape memory alloy, Phase Transit. 81(2008) 537-551.

[28] S.Stupkiewicz, G. Maciejewski, H. Petryk, Low-energy morphology of the interface layer between austenite and twinned martensite, Acta Mater. 55(2007) 6292-6306.

[29] S.Zhang, X. Chen, Z. Moumni, Y. He, Thermal effects on high-frequency magnetic-field-induced martensite reorientation in ferromagnetic shape memory alloys: An experimental and theoretical investigation,Int. J. Plasticity108(2018) 1-20.

[30] S.Zhang, G. Qin, Y.He, Ambient effects on the output strain of Ni–Mn-Ga single crystal magnetic shape memory alloy, J. Alloy Compd. 835(2020) 155-159.

[31] J.M. Ball, K. Koumatos, H. Seiner, Nucleation of austenite in mechanically stabilized martensite by localized heating, J. Alloys Compd. 577(2013) S37-S42.

[32] M.Arndt, M. Griebel, V.Novák, T. Roubíček, P. Šittner, Martensitic transformation in NiMnGa single crystals: Numerical simulation and experiments, Int. J. Plasticity 22(2006) 1943-1961.

[33] K. Haldar, D.C. Lagoudas, I. Karaman, Magnetic field-induced martensitic phase transformation in magnetic shape memory alloys: Modeling and experiments, J. Mech. Phys. Solids. 69(2014) 33-66.

[34] H.E.Karaca, B.Basaran, I. Karaman, Y.I. Chumlyakov, Stress-induced martensite to austenite phase transformation in Ni_2MnGa magnetic shape memory alloys, Smart Mater. Struct. 21(2012)045011.

[35] H.E. Karaca, I. Karaman, B. Basaran, D.C. Lagoudas, Y.I. Chumlyakov, H.J. Maier, On the stress-assisted magnetic-field-induced phase transformation in Ni_2MnGa ferromagnetic shape memory alloys, Acta Mater. 55(2007) 4253-4269.

[36] V.Pinneker, R.Yin, C. Eberl, A. Sozinov, Y. Ezer, M.Kohl, Evolution of local strain bands of different orientation in single crystalline Ni-Mn-Ga foils under tension, J. Alloy Compd. 577(2013) S358-S361.

[37] N.M.Bruno, S. Wang, I. Karaman, Y.I. Chumlyakov, Reversible martensitic transformation under low magnetic fields in magnetic shape memory alloys, Sci. Rep. 7(2017) 40434.

[38] X.Chen, Y.He,Thermo-magneto-mechanical coupling dynamics of magnetic shape memory alloys, Int. J. Plasticity 129(2020) 102686.

[39] X.Chen, Y. He, Z. Moumni, Twin boundary motion in NiMnGa single crystals under biaxial compression, Mater. Lett. 90(2013) 72-75.

[40] X.Chen, Z. Moumni, Y. He, W. Zhang, A three-dimensional model of magneto-mechanical behaviors of martensite reorientation in ferromagnetic shape memory alloys, J. Mech. Phys. Solids 64(2014) 249-286.

[41] Y.J.He, X. Chen, Z. Moumni, Two-dimensional analysis to improve the output stress in ferromagnetic shape memory alloys, J. Appl. Phys. 110(2011) 063905.

[42] Y.J.He, X. Chen, Z. Moumni, Reversible-strain criteria of ferromagnetic shape memory alloys under cyclic 3D magneto-mechanical loadings, J. Appl. Phys. 112(2012)033902.

[43] E.Faran, D. Shilo, Ferromagnetic shape memory alloys — challenges, applications, and experimental characterization, Exp. Techniques 40(2016) 1005-1031.

[44] O. Heczko, A. Sozinov, U. Kari, Giant field-induced reversible strain in magnetic shape memory NiMnGa alloy, IEEE Trans. Magn. 36(2000) 3266-3268.

[45] R.D.James, R.V.Kohn, T.W.Shield, Modeling of Branched Needle Microstructures at the Edge of a Martensite Laminate, J. phys., IV, 05(1995) 253-259.

[46] B.Kiefer, D.C. Lagoudas, Modeling the coupled strain and magnetization response of magnetic shape memory alloys under magnetomechanical loading, J. Intel. Mat. Syst. Str. 20(2008) 143-170.

[47] S.J.Murray, M. Marioni, S.M. Allen, R.C.O'Handley, T.A. Lograsso, 6% magnetic-field-induced strain by twin-boundary motion in ferromagnetic Ni-Mn-Ga, Appl. Phys. Lett. 77(2000) 886-888.

[48] L.Straka, O. Heczko, H.Hänninen, Activation of magnetic shape memory effect in Ni-Mn-Ga alloys by mechanical and magnetic treatment, Acta Mater. 56(2008) 5492-5499.

[49] K.Ullakko, J.K. Huang, C. Kantner, R.C. O'Handly, V.V.Kokorin, Large magnetic field-induced strains in Ni_2MnGa single crystals, Appl. Phys. Lett. 69(1996) 1966.

[50] C.Yu,T. Chen, H.Yin, G.Kang, D. Fang, Modeling the anisotropic elastocaloric effect of textured NiMnGa ferromagnetic shape memory alloys, Int. J. Solids Struct, 191-192(2020) 509-528.

[51] S. Zhang, X. Chen, Z. Moumni, Y. He, Coexistence and compatibility of martensite reorientation and phase transformation in high-frequency magnetic-field-induced deformation of Ni-Mn-Ga single crystal, Int. J. Plasticity 110 (2018) 110-122.

[52] O.Heczko, N. Lanska, O.Soderberg, K. Ullakko, Temperature variation of structure and magnetic properties of Ni-Mn-Ga magnetic shape memory alloys, J. Magn. Magn. Mater. 242-245(2002) 1446-1449.

[53] O.Z. Pascan, Y He, Z. Moumni, W Zhang, Temperature rise of high-frequency martensite reorientation via Type II twin boundary motion in NiMnGa Ferromagnetic Shape Memory Alloy, Scripta Mater. 104(2015) 71-74.

[54] L. Straka, O. Heczko, H. Seiner, N. Lanska, J. Drahokoupil, A. Soroka, S. Fähler, H. Hänninen, A. Sozinov, Highly mobile twinned interface in 10M modulated Ni-Mn-Ga martensite: Analysis beyond the tetragonal approximation of lattice, Acta Mater.59(2011)7450-7463.

[55] R. Chulist, L. Straka, N. Lanska, A. Soroka, A. Sozinov, W. Skrotzki, Characterization of mobile type I and type II twin boundaries in 10M modulated Ni-Mn-Ga martensite by electron backscatter diffraction,Acta Mater. 61(2013)1913-1920.

[56] O. Heczko, L. Straka, H. Seiner, Different microstructures of mobile twin boundaries in 10M modulated Ni-Mn-Ga martensite, Acta Mater. 61 (2013) 622-631.

[57] Bronstein E., Faran E., Shilo D.,.Analysis of austenite-martensite phase boundary and twinned microstructure in shape memory alloys: The role of twinning disconnections, Acta Mater.164 (2019) 520-529.

[58] N. M. Bruno, C. Ciocanel, H. P. Feigenbaum, A. Waldauer, A theoretical and experimental investigation of power harvesting using the NiMnGa martensite reorientation mechanism, Smart Mater. Struct. 21 (2012) 094018.

[59] E.Faran, D.Shilo, The kinetic relation for twin wall motion in NiMnGa, J. Mech. Phys. Solids 61 (2011) 975-987.

[60] C. Zhang, G. Qin, S. Zhang, X. Chen, Y. He, Hysteresis effect on austenite-martensite interface in Ni-Mn-Ga single crystal, Scripta Mater.222 (2023) 115029.

[61] G.Ruddock, A microstructure of martensite which is not a minimiser of Energy: the X-interface, Arch. Rational Mech. Anal. 127(1994) 1-39.

[62] H. Seiner, P. Sedlák and M. Landa, Shape recovery mechanism observed in single crystals of Cu-Al-Ni shape memory alloy, Phase Transit. 81(2008)537-551.

[63] H. Seiner and M. Landa, Non-classical austenite-martensite interfaces observed in single crystals of Cu-Al-Ni, Phase Transit. 82 (2009)793-807.

[64] D. C. Lagoudas, P. B. Entchev, P. Popov, E. Patoor, L. C. Brinson, X. Gao, Shape memory alloys, Part II: Modeling of polycrystals, Mech. Mater. 38 (2006) 430-462.

[65] Y. Aydogdu, A. Aydogdu, O. Adiguzel, Self-accommodating martensite plate variants in shape memory CuAlNi alloys,J. Mater. Process. Tech. 123 (2002) 498-500.

[66] S. Miyazaki, K. Otsuka, C. M. Wayman, The shape memory mechanism associated with the martenstic transformation in Ti-Ni alloys-I Self-accommodation, Acta metall. 37(1989)1873-1884.

[67] C. M. Wayman, Shape memory and related phenomena, Prog. Mater. Sci. 36 (1992) 203-224.

[68] A. Diestel, V. Neu, A. Backen , L. Schultz, S. Fahler, Magnetic domain pattern in hierarchically twinned epitaxial Ni–Mn–Ga films, J. Phys.: Condens. Matter 25 (2013) 266002.

[69] J. N. Armstrong, M. R. Sullivan, M. Le Romancer, V. A. Chernenko, H. D. Chopra, Role of magnetostatic interactions in micromagnetic structure of multiferroics, J. Appl. Phys. 103 (2008) 023905.

[70] A. Neudert, Y. W. Lai, R. Schafer, M. Kustov, L. Schultz, J. McCord, Magnetic domains and twin boundary movement of NiMnGa magnetic shape memory crystals, Adv. Eng. Mater. 14 (2012) 601.

[71] Q. Peng, Y.J. He, Z. Moumni, A phase-field model on the hysteretic magneto-mechanical behaviours of ferromagnetic shape memory alloy, Acta Mater. 88(2015) 13-24.

[72] K. Bhattacharya, Microstructure of Martensite: Why it Forms and How it Gives Rise to the Shape-memory Effect, Oxford University Press, Oxford, 2003.

[73] K. Bhattacharya, Self-accommodation in martensite, Arch. Ration. Mech. Anal.120 (1992) 201–244.

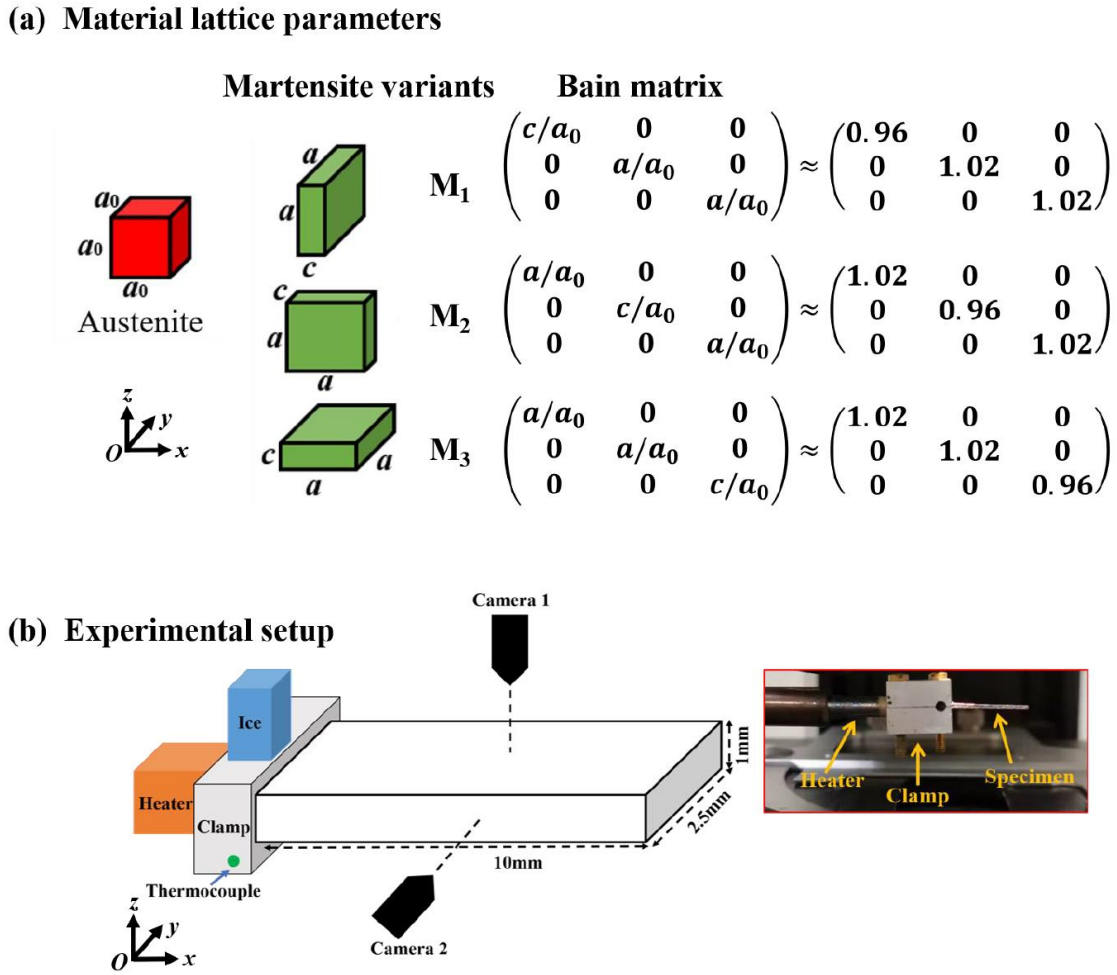

Fig. 1(a) The material is cubic austenite phase at high temperature and tetragonal martensite phase at low temperature (the three martensite variants M_1, M_2 and M_3 have their short axes along the *x*-, *y*- and *z*-direction, respectively); (b) Experimental setup: a specimen is clamped at one end and the other end is free to deform.

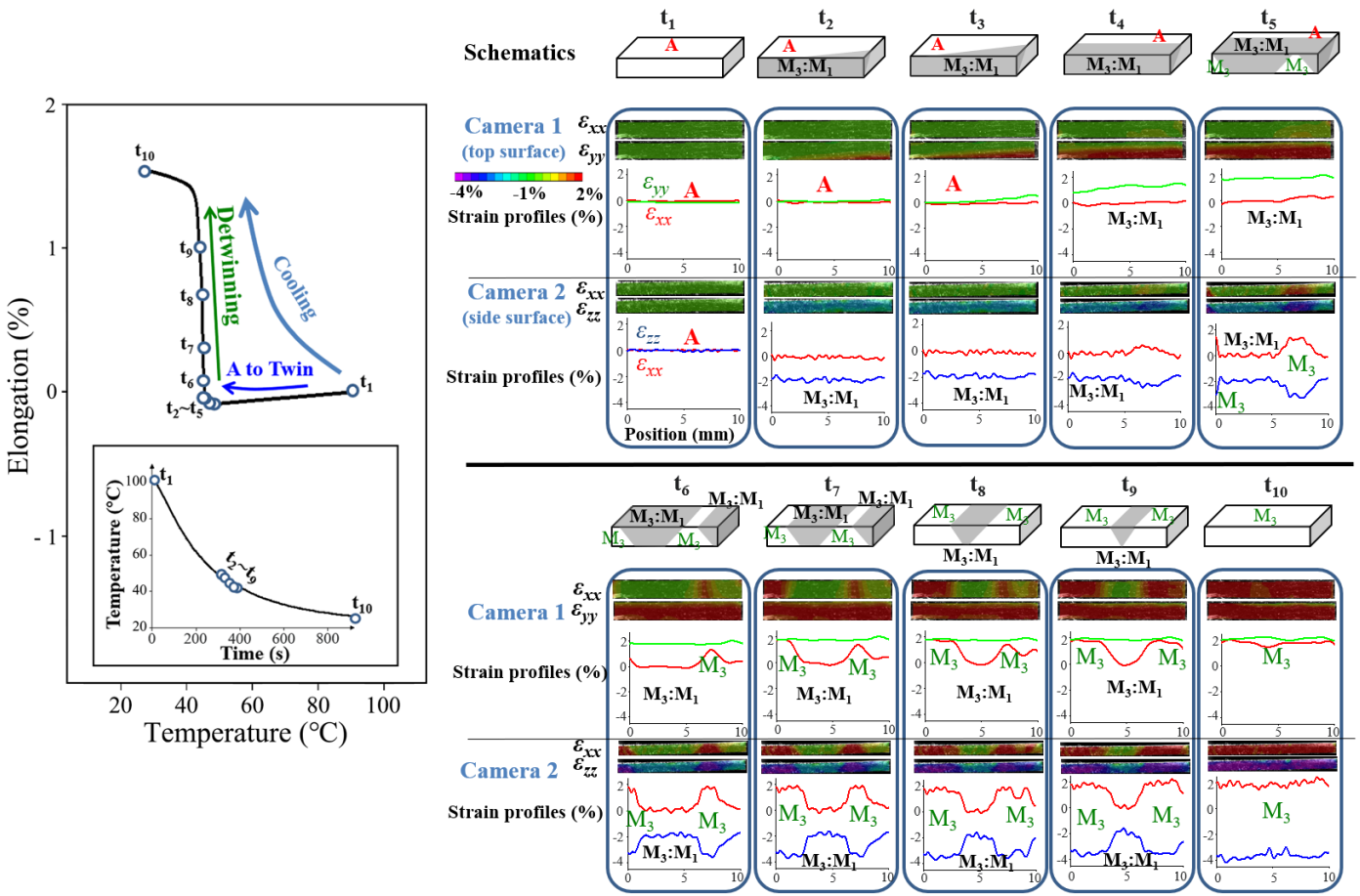

Fig. 2 The specimen's global elongation and the local strain evolution (DIC strain maps and the typical strain profiles along the specimen's length direction at the specimen's middle line) during the natural cooling of CTS (Complete Transformation System with strong heating). The A→M transformation was via two steps: A→twin M_3:M_1 (with volume ratio 2:1) and the detwinning into the single variant M_3. The specimen's global elongation was mainly due to the detwinning at $t_5 \sim t_{10}$. The symbols $t_1 \sim t_{10}$ represent the time moments of the thermal loading indicated by the temperature-time curve on the left-hand side of the figure.

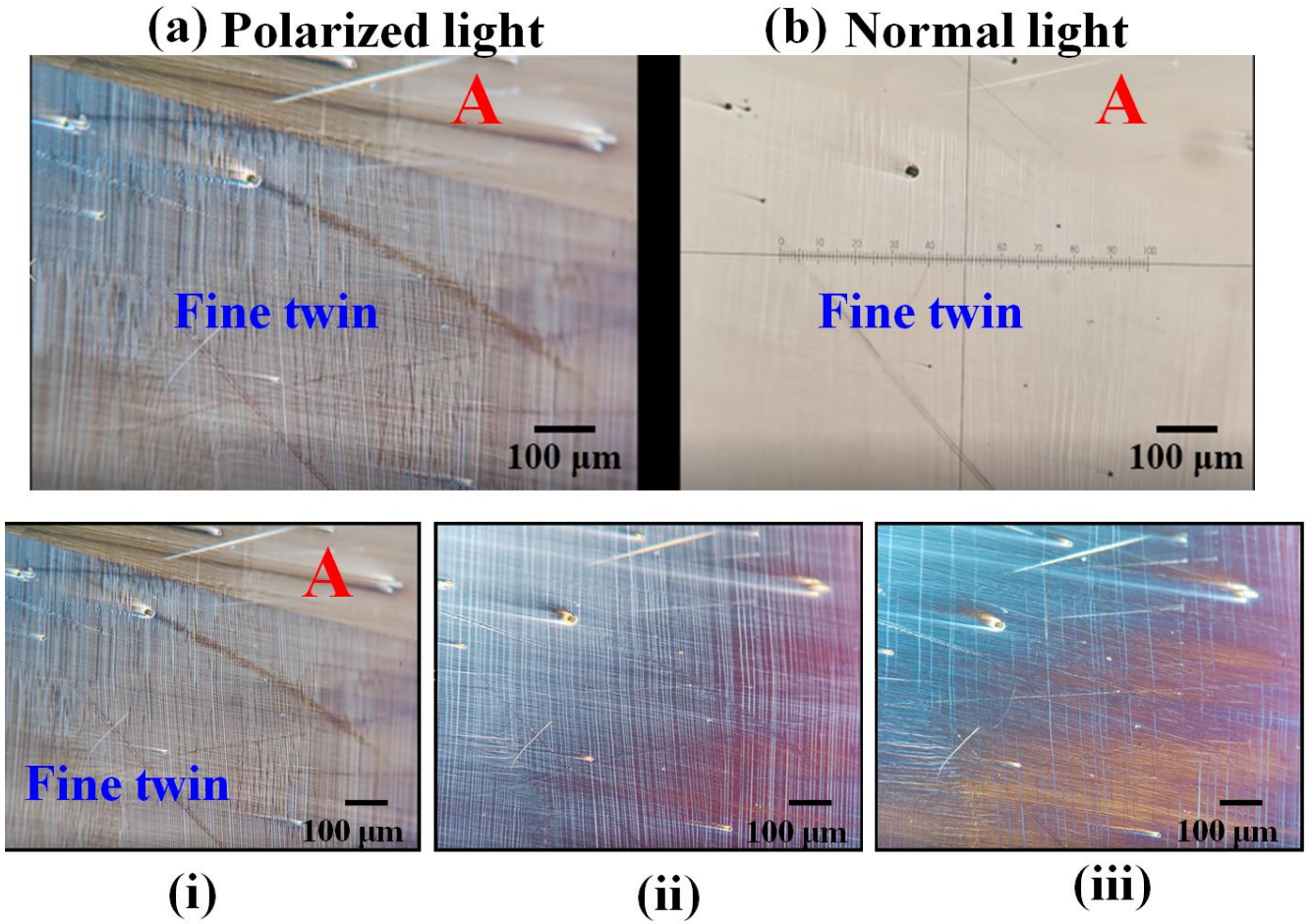

Fig. 3 The spontaneous detwinning can be better captured by the microscope with polarized light (a) than with normal light (b). Typical frames from Movie 1 of the supplementary materials: (i) Coexistence of austenite and martensite twin laminates (ii) Evolving twin (twin boundaries intermittently disappear); (iii) A single martensite variant dominates.

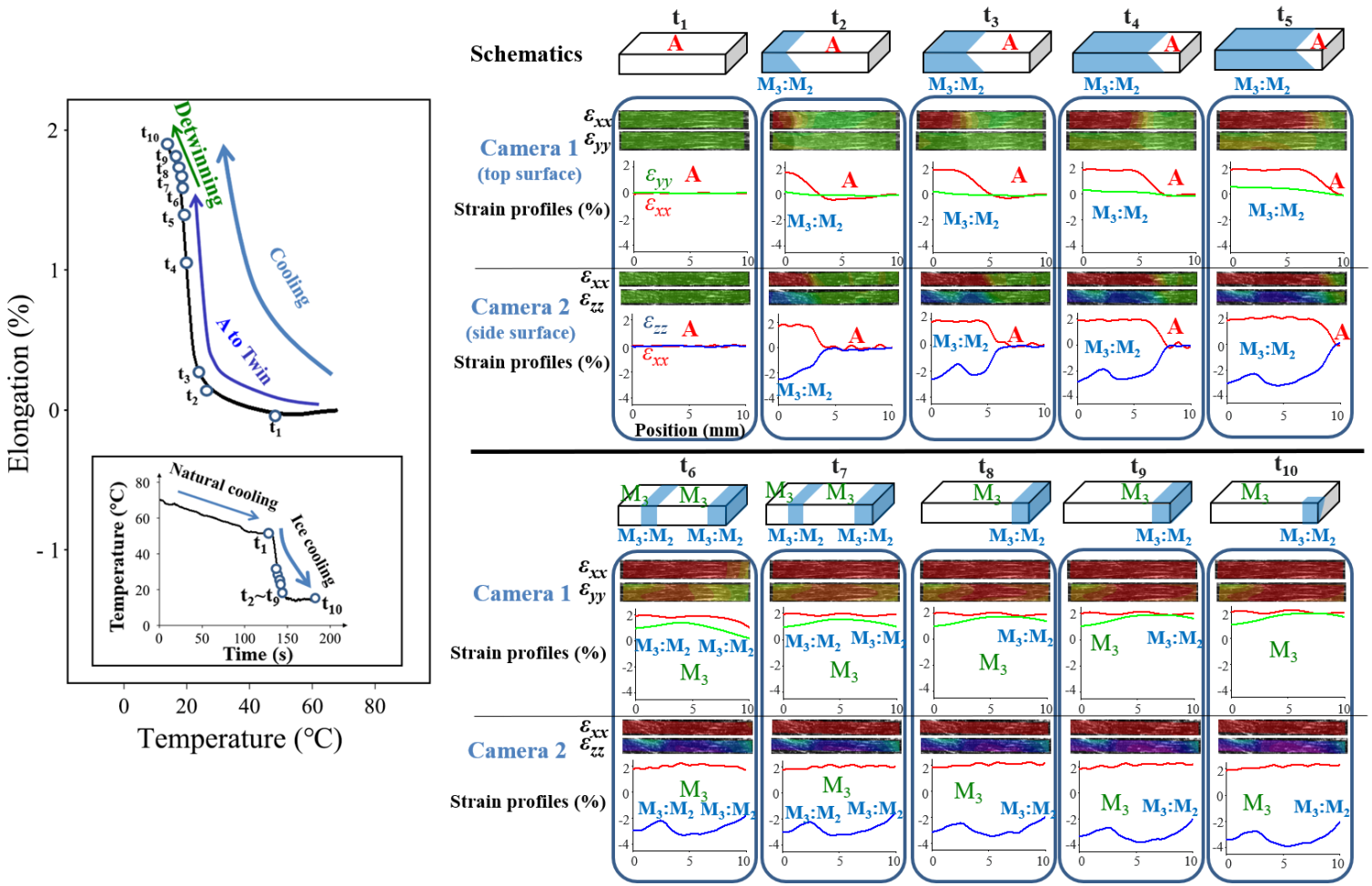

Fig. 4 The specimen's global elongation and the local strain evolution during the ice cooling of the CTS (Complete Transformation System with strong heating). The A→M transformation was via two steps: A→twin M_3:M_2 (with volume ratio 2:1) and the detwinning into the single variant M_3. The specimen's global elongation was mainly due to the A→twin transformation. The symbols t_1 ~ t_{10} represent the time moments of the thermal loading indicated by the temperature-time curve on the left-hand side of the figure.

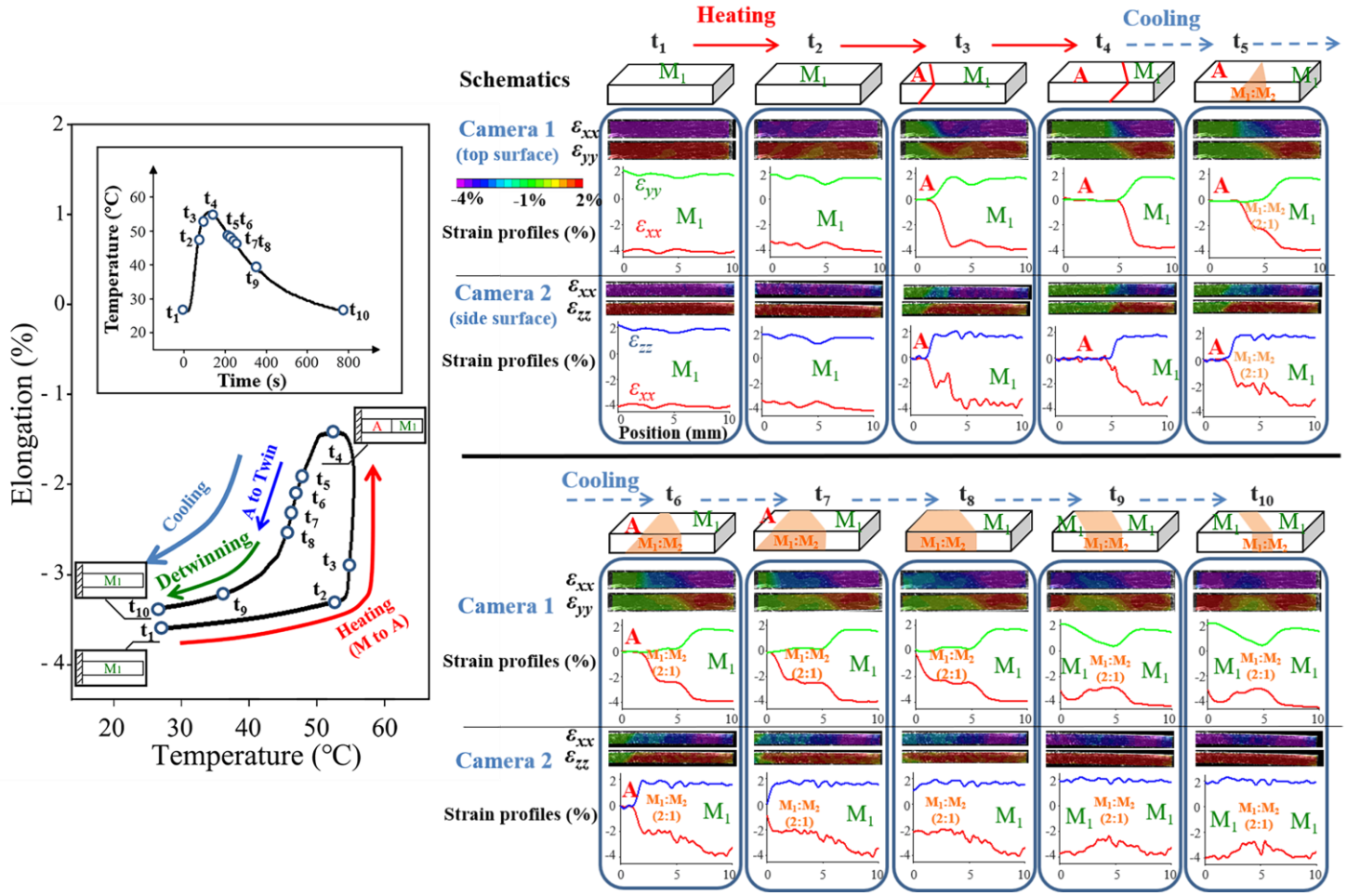

Fig. 5 Heating-cooling cycle of ITS (Incomplete Transformation System) with the initial martensite state of the single variant M_1. The transition zone consisting of the twin M_1:M_2 (with the volume ratio 2:1) between A-phase and M_1 was clearly captured during the cooling process.

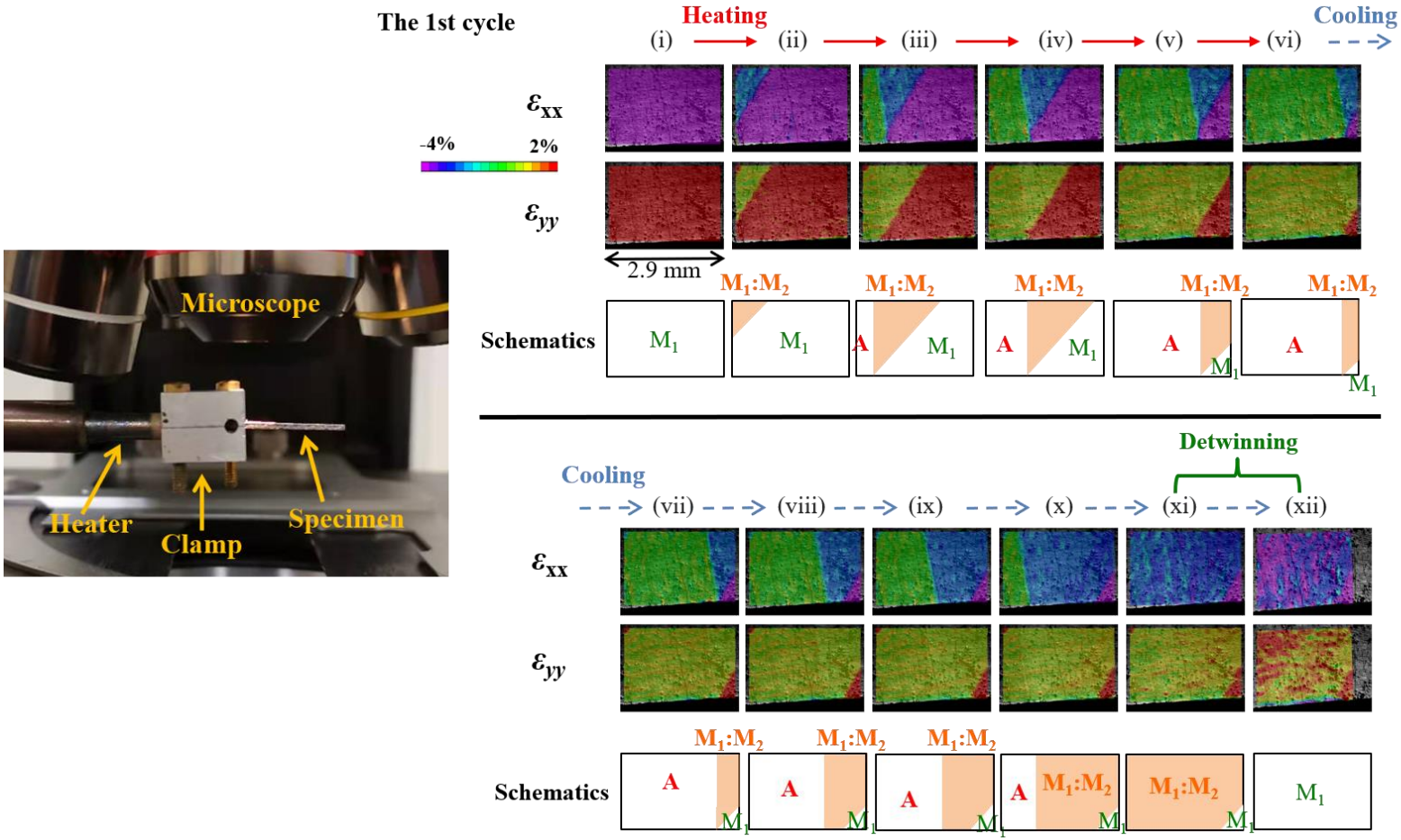

Fig. 6 The observation by the microscope (in terms of DIC strain maps) on the local strain evolution during the 1st cycle of the three continuous heating-cooling cycles of ITS (Incomplete Transformation System) with the initial martensite state M_1. A small transition zone of the twin M_1:M_2 (volume ratio 2:1) separating A-phase from M_1 during the heating process; then the transition zone grew up and was detwinned into M_1 during the cooling process.

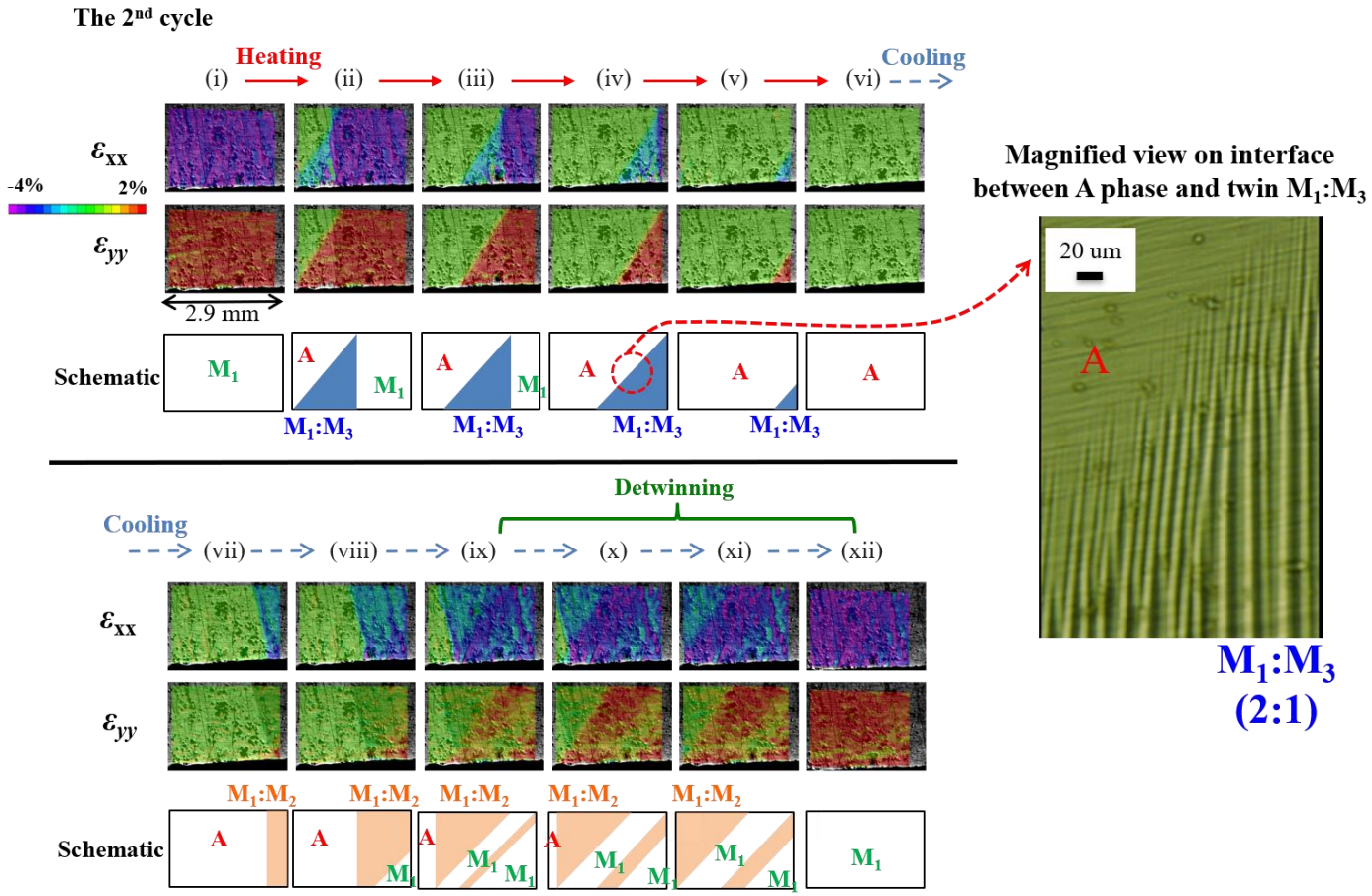

Fig. 7 The observation by the microscope on the local strain evolution during the 2nd cycle of the three continuous heating-cooling cycles of ITS (Incomplete Transformation System) with the initial martensite state M_1. A small transition zone of twin M_1:M_3 (volume ratio 2:1) separated A-phase from M_1 during the heating process; the transition zone consisted of a laminate of the twin as shown by the magnified view. During the cooling process, a different twin was formed (M_1:M_2), grew up and was detwinned into M_1.

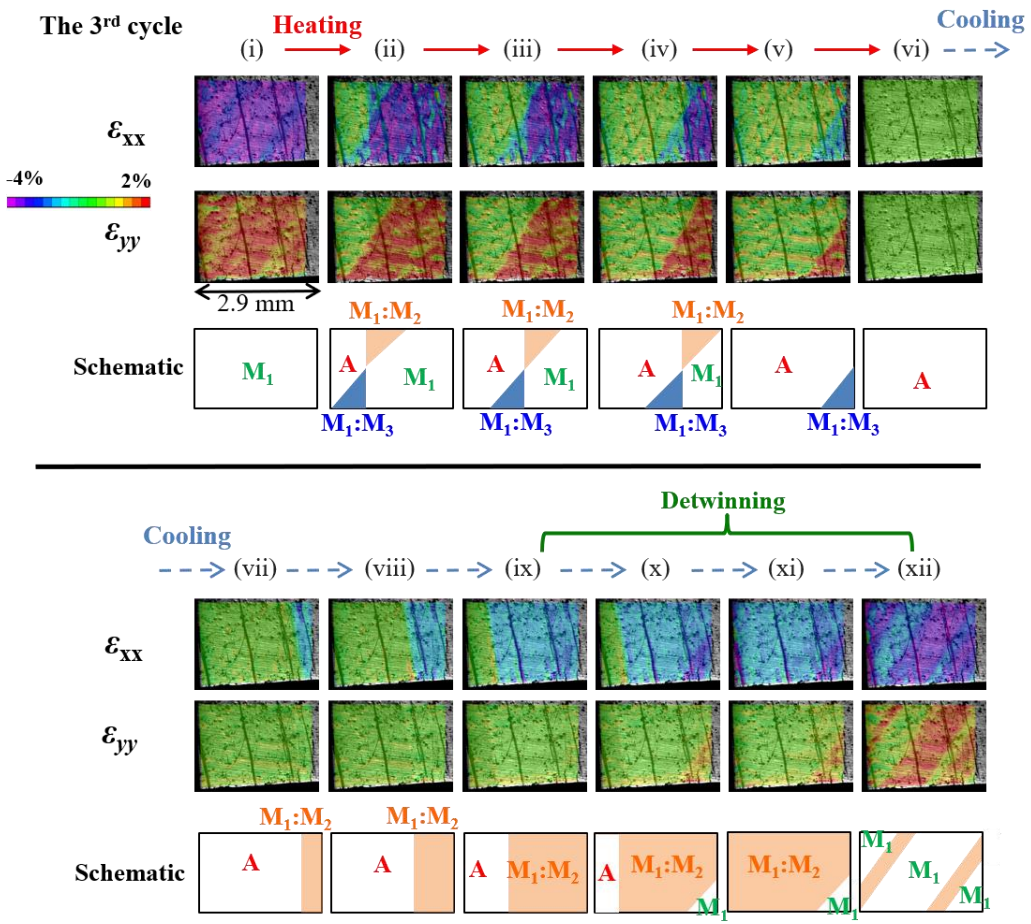

Fig. 8 The observation by the microscope on the local strain evolution during the 3rd cycle of the three continuous heating-cooling cycles of ITS (Incomplete Transformation System) with the initial martensite state M_1. An "X" type A-M interface consisting of two different transition zones (twins M_1:M_2 and M_1:M_3) were formed during the heating process. During the cooling process, there was only one transition zone of the twin (M_1:M_2) that grew up and was detwinned into M_1.

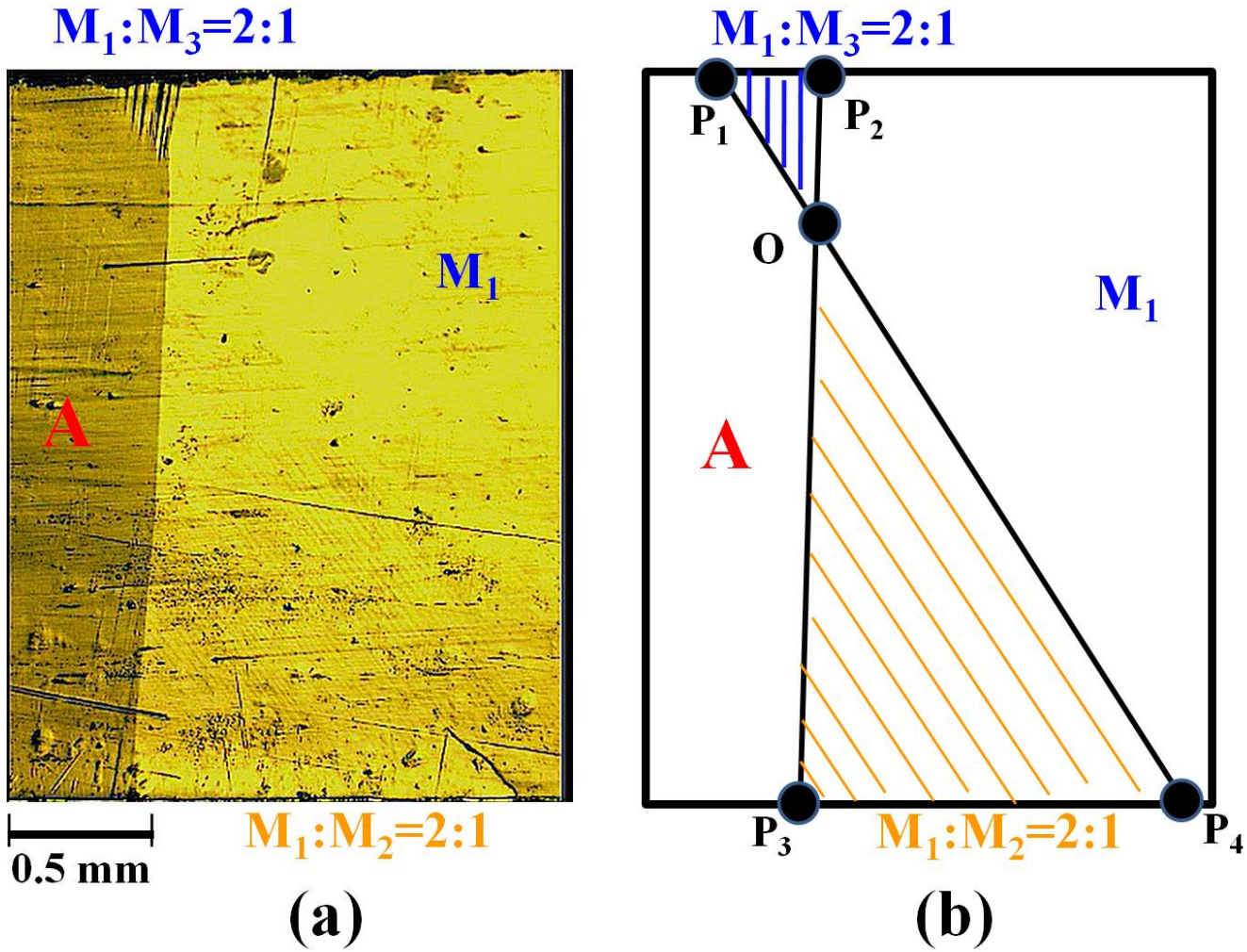

Fig. 9 The microscope observation (a) (from Movie 2 in supplementary materials) and the schematic (b) of the X-type A-M interface and the associated twin laminates.

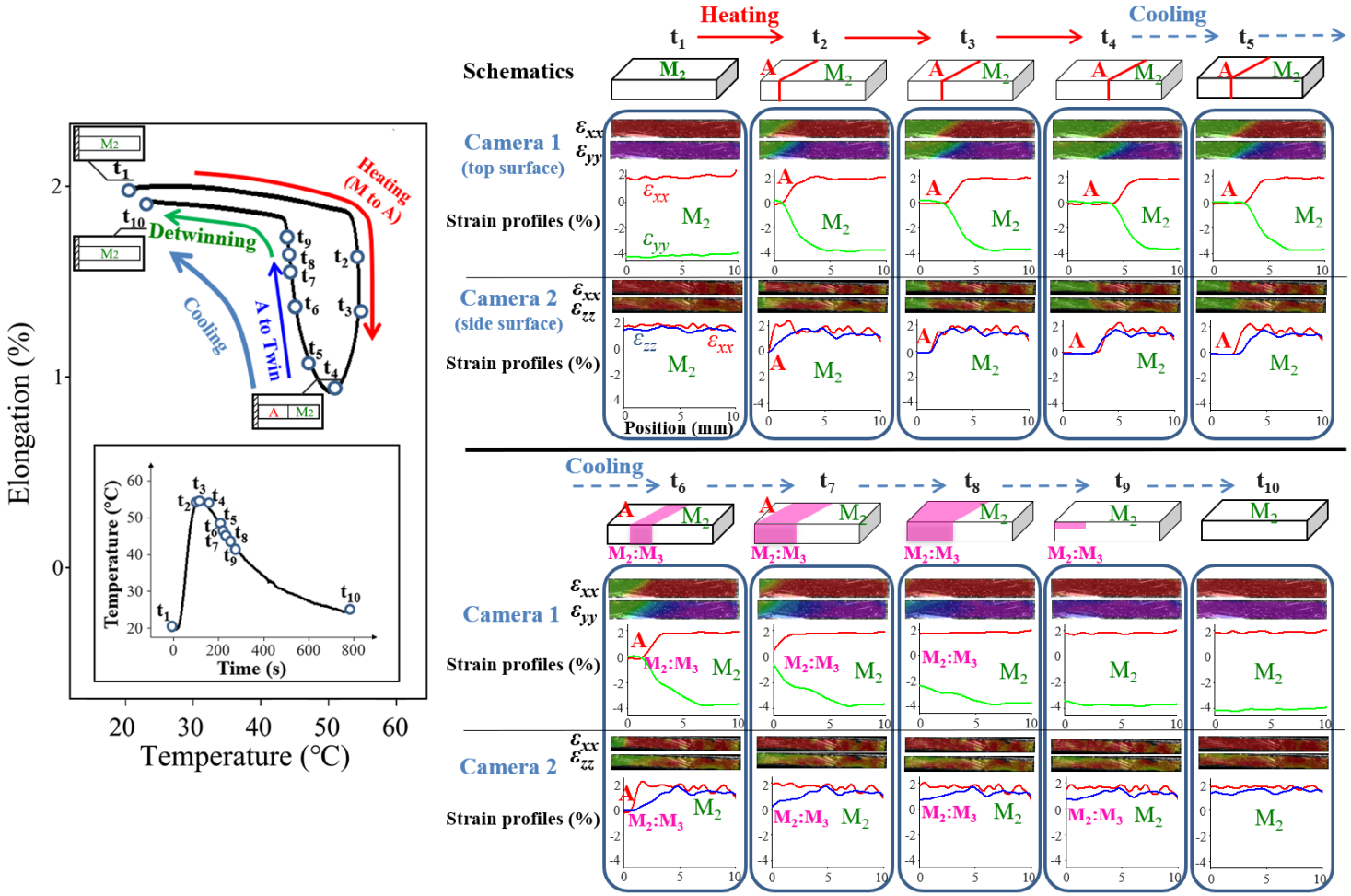

Fig. 10 The specimen's global elongation and the local strain evolution during the heating-cooling cycle of ITS (Incomplete Transformation System) with the initial martensite state of M_2. The heating-cooling cycle led to the cyclic A-M phase transformation with a significant cyclic deformation and the single variant M_2 occupied the specimen at both the initial and final states of the cycle.

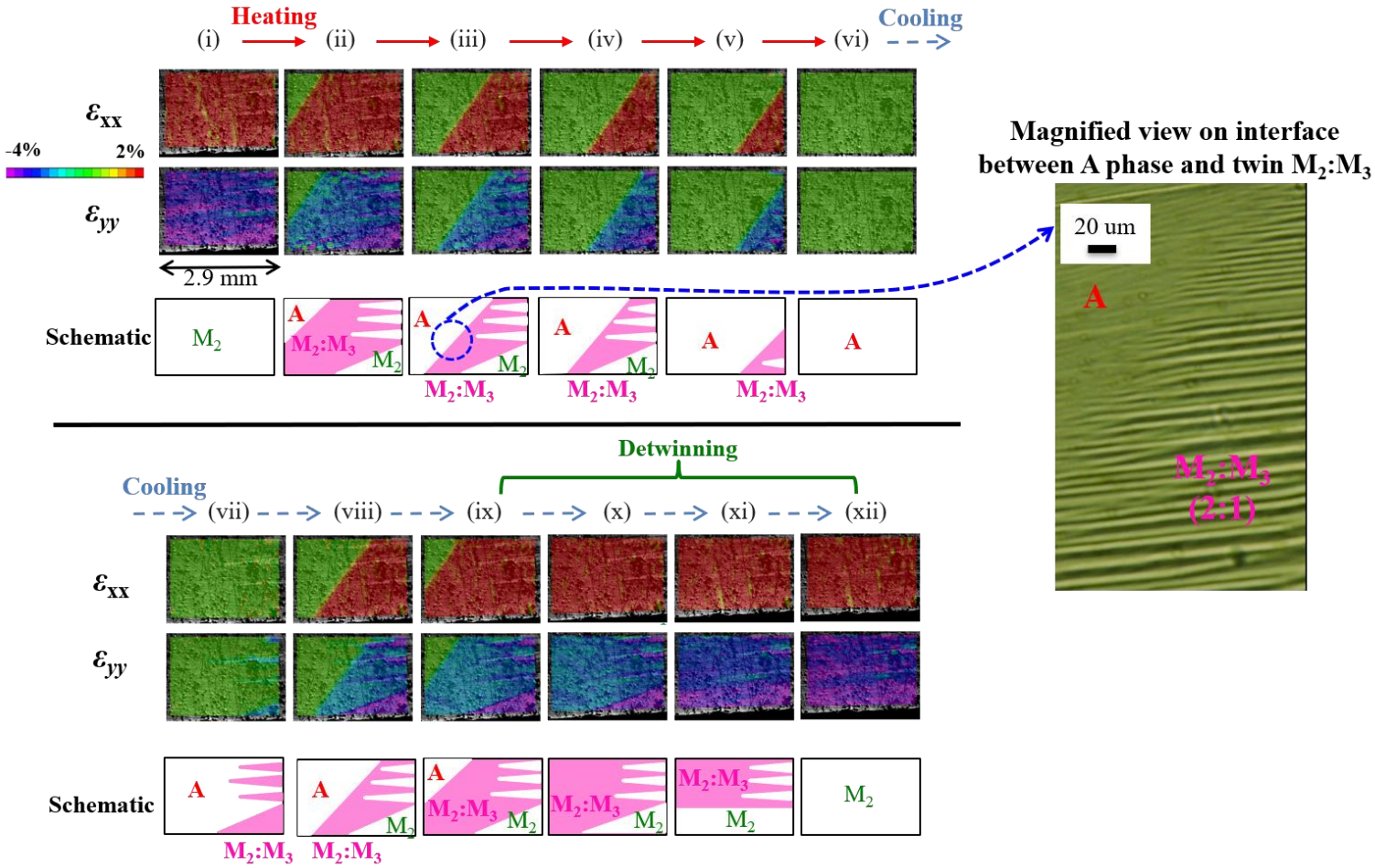

Fig. 11 The observation by the microscope on the local strain evolution during the heating-cooling cycle of ITS (Incomplete Transformation System) with the initial martensite state of M_2. The transition zone consisting of the twin M_2:M_3 (with volume ratio 2:1) had a fine-needle pattern near the region of A-phase (shown by the magnified view) and a coarse-arrow pattern near the region of M_2.

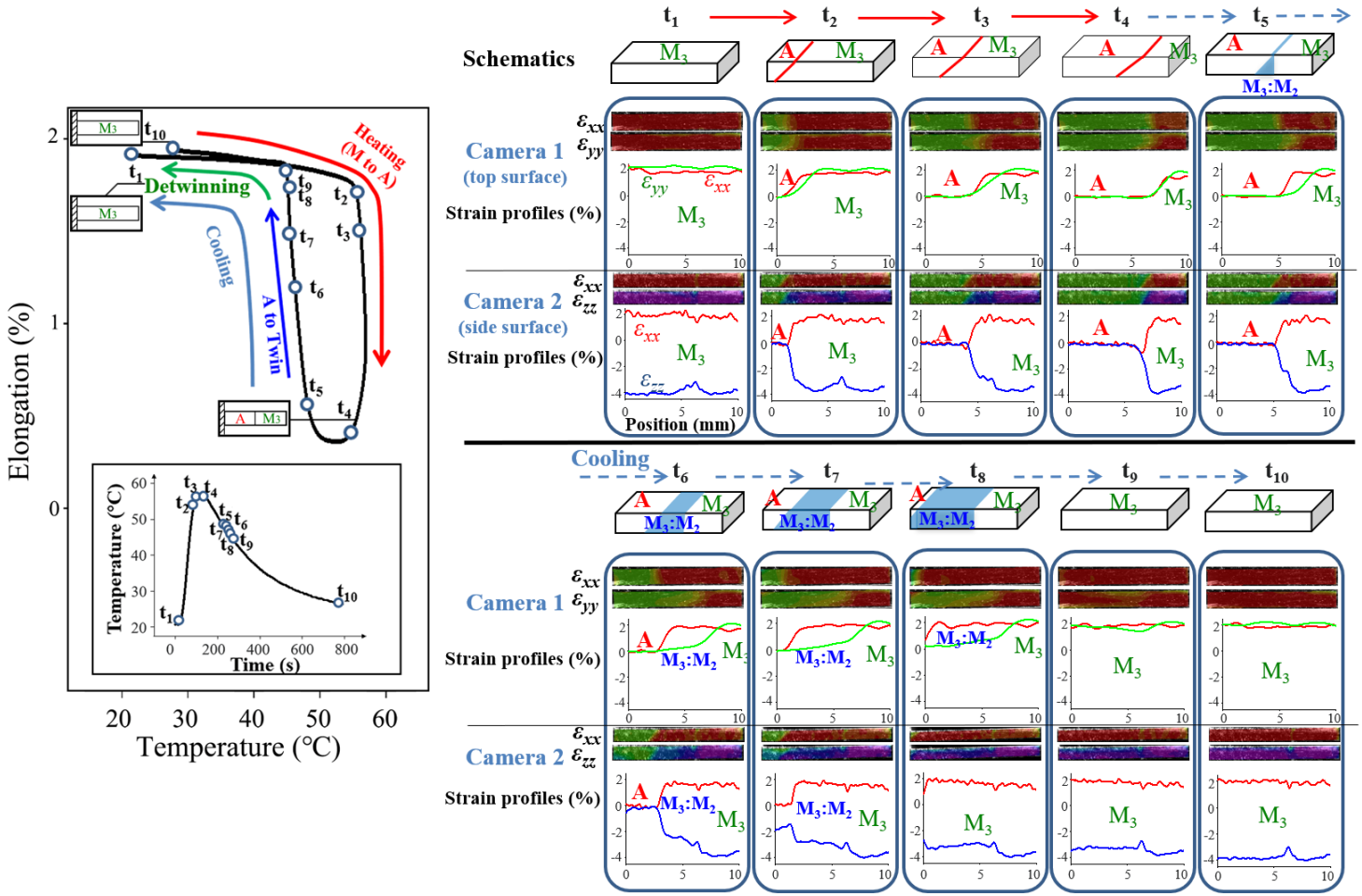

Fig. 12 The specimen's global elongation and the local strain evolution during the heating-cooling cycle of ITS (Incomplete Transformation System) with the initial martensite state of M_3. The transition zone of the twin M_3:M_2 (with volume ratio 2:1) was clearly captured during the cooling process. The heating-cooling cycle led to the cyclic A-M phase transformation with a significant cyclic deformation and the single variant M_3 occupied the specimen at both the initial and final states of the cycle.

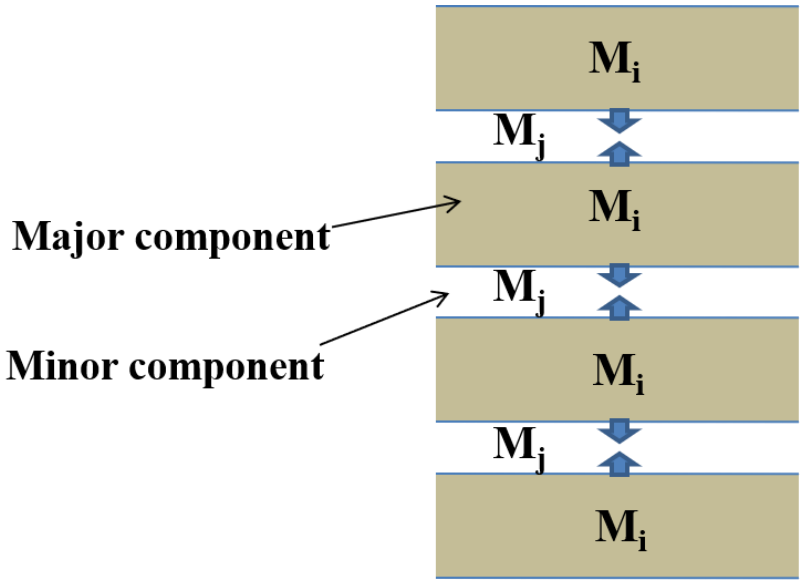

Fig. 13 The schematic of spontaneous detwinning: the nearest neighbouring twin boundaries move to each other, merge together and finally disappear, leaving the whole region occupied by the major component (the state of single martensite variant M_i).

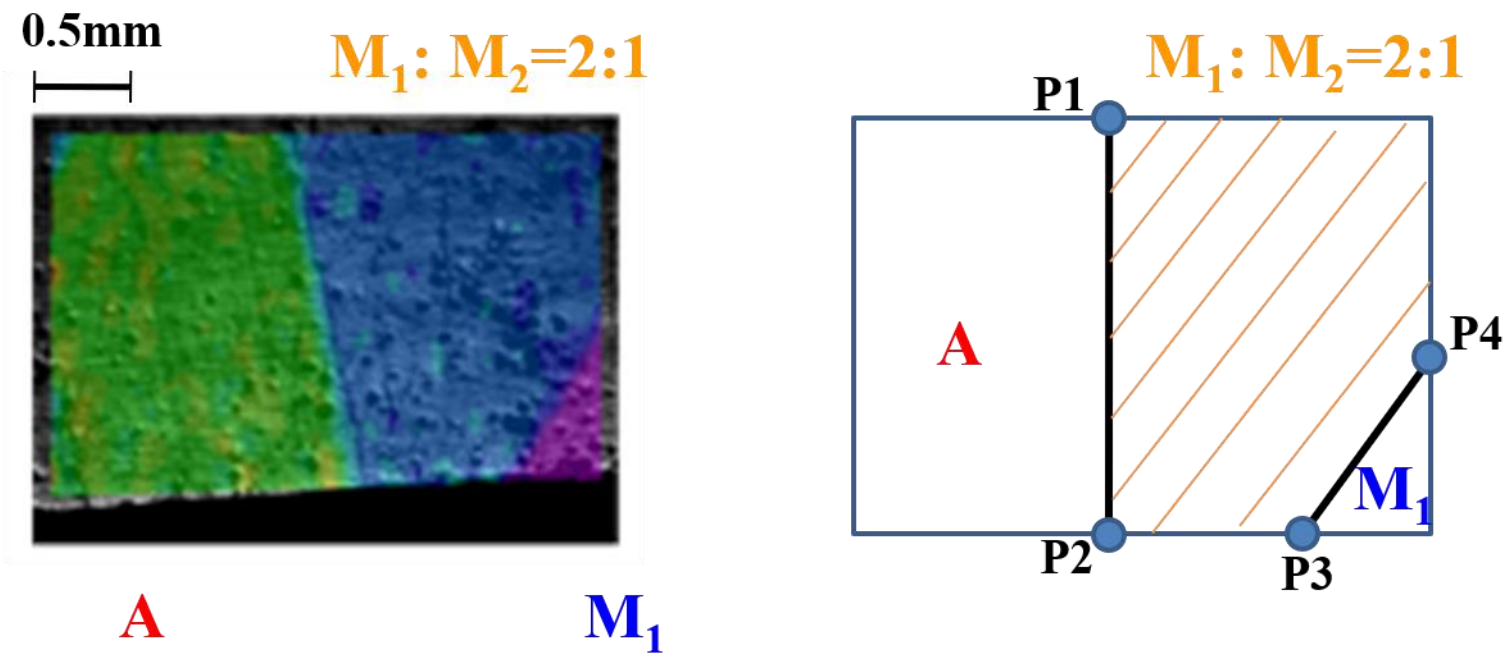

Fig. 14 Example of a twin compatibly separating the A-phase from the single martensite variant.

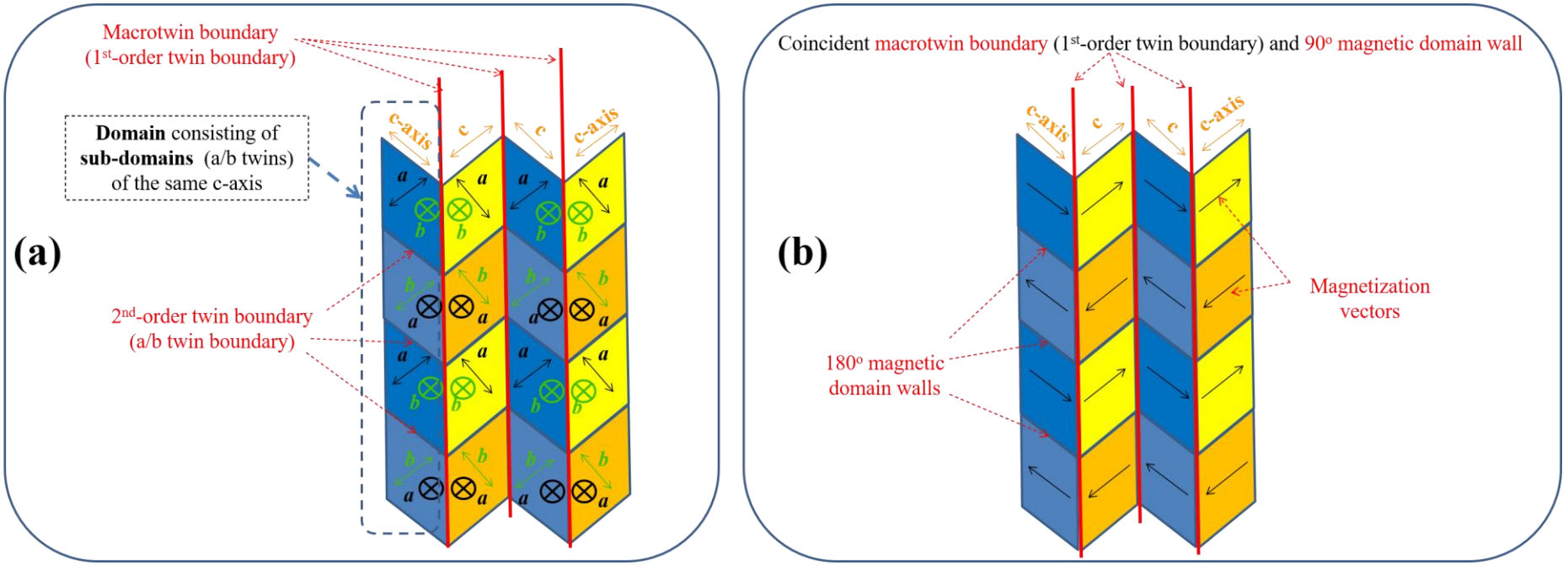

Fig. 15 Schematics of multiscale martensite structure (a) and the magnetic domains embedded in twins (b).